Atmospheric Research 122 (2013) 111–135

Contents lists available at SciVerse ScienceDirect

Atmospheric Research

journal homepage: www.elsevier.com/locate/atmos

An evaluation of a semi-analytical cloud property retrieval using MSG SEVIRI, MODIS and CloudSat

Meike Kühnlein [a,*], Tim Appelhans [a], Boris Thies [c], Alexander A. Kokhanovsky [b], Thomas Nauss [a]

[a] Environmental Informatics, Faculty of Geography, Philipps-University Marburg, Marburg, Germany
[b] Institute of Environmental Physics, Bremen University, O. Hahn Allee 1, 28334 Bremen, Germany
[c] Laboratory for Climatology and Remote Sensing, Faculty of Geography, Philipps-University Marburg, Marburg, Germany

ARTICLE INFO

Article history:
Received 21 April 2012
Received in revised form 15 October 2012
Accepted 24 October 2012

Keywords:
Cloud properties
Satellite retrieval
SLALOM
MSG SEVIRI
CloudSat
MODIS

ABSTRACT

Knowledge of cloud properties such as cloud effective radius (a_{ef}) and optical thickness (τ) is essential to understand their role in the dynamic radiation budget and climate change. The Spinning Enhanced Visible and Infrared Instrument (SEVIRI) on board Meteosat Second Generation (MSG) with its high temporal resolution (15 min), permits a quasi-continuous monitoring of the evolution of cloud properties. This has motivated the adaptation of the SLALOM (SimpLe Approximations for cLOudy Media) algorithm, a semi-analytical cloud property retrieval technique to MSG SEVIRI. The optical properties retrieved by SLALOM are compared against the well known and validated NASA MODIS cloud property product (MODIS 06) as well as the cloud optical depth product (2B-TAU) of CloudSat. The results are shown over the North Atlantic and over the European continent with the intention of determine the relative accuracy between SLALOM and the other retrievals. Over the North Atlantic, SLALOM-based cloud properties retrieved from SEVIRI datasets show a good agreement with the MODIS 06 product with correlation coefficients of 0.93 (τ) and 0.82 (a_{ef}). The largest deviations were found in less homogeneous cloud areas that are characterized by broken clouds and toward the cloud borders. Moreover, SLALOM optical thickness values are well within the range of corresponding CloudSat 2B-TAU optical thickness values which can be found within a SEVIRI pixel, except for $\tau<5$ where SLALOM tends to overestimate τ. Despite the different sensor characteristics and viewing geometries, the retrieved cloud properties compare very well. Over Europe, the evaluation between SLALOM and MODIS 06 showed larger differences. We attribute this to (a) uncertainties related to the surface albedo which is treated differently in the algorithms and is based on different albedo maps and (b) inhomogeneities of clouds which exhibit quite complex structures particularly over land. The latter are detected on different scales by MODIS and SEVIRI because of their different spatial resolutions. Given the demonstrated accuracy of SLALOM using MSG SEVIRI data there is a wide spread of potential applications.

1. Introduction

Clouds play an important role in the Earth's climate system (Liou, 1992; Platnick and Valero, 1995; Stephens, 2005) and are recognized as a key modifier of the earth-atmosphere radiation budget (Kiehl and Trenberth, 1997) driving atmospheric dynamics, hydrological cycle and global warming. The radiative properties of clouds and hence their influence on the earth-atmosphere radiation budget can largely be explained by a few optical and microphysical cloud parameters, particularly the cloud optical thickness and the effective cloud droplet radius. Despite their great importance, the correct spatio-temporal measurement of clouds is still associated with large uncertainties (Stephans et al., 2007). This is mainly due to the fact that clouds are characterized by a highly short-lived nature. However, detailed information about clouds are important for

* Corresponding author at: Philipps-University Marburg, 35037 Marburg, Germany. Tel.: +49 6421 2825954; fax: +49 6421 2825670.
E-mail address: meike.kuehnlein@staff.uni-marburg.de (M. Kühnlein).

0169-8095/$ – see front matter © 2012 Elsevier B.V. All rights reserved.
http://dx.doi.org/10.1016/j.atmosres.2012.10.029

a better understanding of the climate system. The possibility to obtain information about cloud properties and their spatial distribution on a global scale can be achieved by satellite remote sensing only.

Over the past decades, various algorithms have been developed to retrieve optical and microphysical cloud properties (e.g. Arking and Childs, 1985; Han et al., 1994; Kawamoto et al., 2001; Kokhanovsky et al., 2003; Kokhanovsky and Nauss, 2005; Liou and Wittman, 1979; Nakajima and King, 1990; Nakajima and Nakajima, 1995; Nauss and Kokhanovsky, 2011; Platnick et al., 2003; Roebeling et al., 2006; Strabala et al., 1994; Twomey and Cocks, 1982). The performance of many cloud retrieval algorithms using satellite data from passive imager instruments is being evaluated by Eumetsat's cloud retrieval evaluation workshop (CREW, see http://www.icare.univ-lille1.fr/crew/). Long time series of such and other satellite derived cloud properties are retrieved by the Working Group on Data Management and Analysis (WGDMA) of the International Satellite Cloud Climatology Project (ISCCP) as part of the World Climate Research Program (WCRP) (Schiffer and Rossow, 1983; Rossow, 1989; see http://isccp.giss.nasa.gov/index.html) as well as the MODIS cloud product team at NASA (Platnick et al., 2003, see http://modis-atmos.gsfc.nasa.gov/MOD06_L2/index.html).

For day-time observations, these techniques rely on the concurrent measurement of the cloud reflectance in absorbing and non-absorbing wavelengths. The reflection of clouds in the visible region strongly depends on cloud optical thickness, whereas the reflection in the near-infrared region is additionally related to the cloud droplet size (i.e. effective cloud droplet radius, see e.g. integrative figure in Nakajima and King, 1990). The majority of the retrieval techniques have been developed for optical sensors aboard polar-orbiting satellites mainly because of the available spectral resolution. Up until now, only a few techniques are applied to geostationary satellite systems (e.g. Feijt et al., 2004; Han et al., 1994; Pandey et al., 2012; Pérez et al., 2011; Roebeling et al., 2006, 2008).

The present European geostationary system Meteosat Second Generation (MSG), carrying the Spinning Enhanced Visible and Infrared Instrument (SEVIRI, Aminou, 2002), provides sufficient spectral resolution required for cloud retrievals. Furthermore, its relatively high spatial (3 by 3 km at sub satellite point) and very high temporal resolution (15 min) permits a quasi-continuous monitoring of the evolution of cloud properties which is of particular importance with respect to the spatio-temporal cloud cover dynamics. Recently, Nauss and Kokhanovsky (2011) developed SLALOM (SimpLe Approximations for cLOudy Media), a cloud property retrieval based on approximations of the asymptotic solutions of the radiative transfer theory using data from the Moderate Resolution Imaging Spectroradiometer (MODIS). The computation speed and accuracy of this retrieval along with the enhanced information

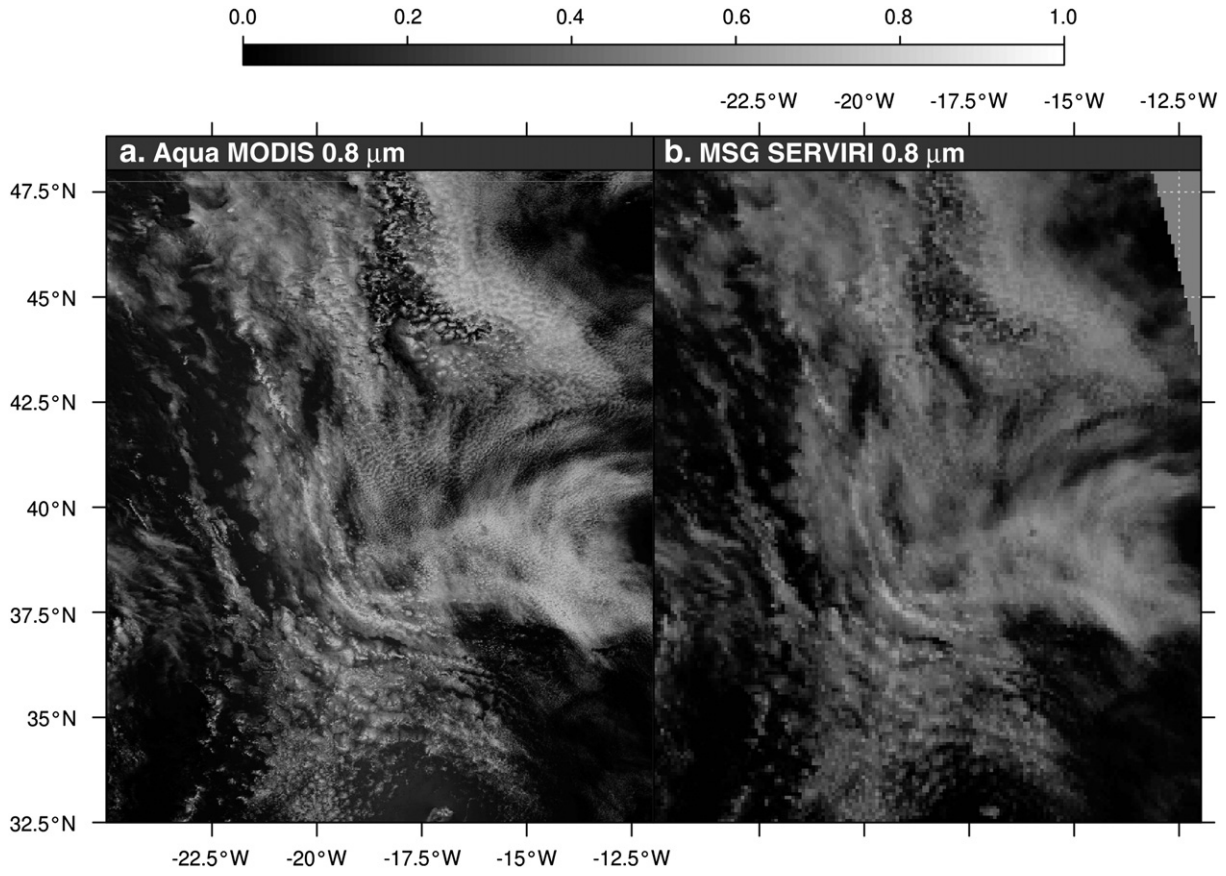

Fig. 1. (a) Aqua MODIS and (b) MSG SEVIRI 0.8 μm reflectances over the North Atlantic for 11 June 2008 14:15 and 14:20 UTC (Aqua MODIS: 0.01°×0.01°, MSG SEVIRI: 0.08°×0.08°).

content potentially provided by the spatio-temporal high resolution geostationary data motivates the adaptation of the SLALOM algorithm to MSG SEVIRI.

In this study, SEVIRI and MODIS-based results of SLALOM will be compared to the LUT-based approach by Platnick et al. (2003) for the MODIS sensor on-board of the NASA EOS Aqua and Terra satellites (King and Greenstone, 1999) and the cloud optical depth product (2B-TAU) of CloudSat (Polonsky et al., 2008). The validation against CloudSat 2B-Tau product is of great value, since CloudSat serves, based on the detailed information about the vertical structure of the cloud measured by its Cloud Profiling Radar (CPR), a quantitative basis to produce an accurate cloud optical depth profile which forms a very good validation source. Furthermore, CloudSat 2B-Tau provides detailed information on the sub-pixel heterogeneity of the cloud structure within the larger SEVIRI pixel. So far, CloudSat measurements have been used only in a few studies for the validation of cloud retrievals (e.g. Bennartz et al., 2010; Pandey et al., 2012; Pérez et al., 2011). Unfortunately, existing retrieval algorithms applied to geostationary satellite systems are either not yet available to the public or have yet to be adapted to existing processing chains and therefore could not used for the evaluation.

While idealized radiative transfer measurements could be used to evaluate the theoretical accuracy of a retrieval or as an alternative data source for within sensor evaluation set-ups, across-sensor studies show the performance under real conditions and provide an estimate for the uncertainties which must be expected if data from different sources is analyzed within the respective studies.

The algorithms presented in this study are capable of retrieving many other cloud parameters like liquid and ice water path and particle absorption length, but only results of effective radius and optical thickness are compared. Furthermore, only the case of liquid clouds is considered since the complexity of light transport through highly inhomogeneous crystalline clouds bears many intrinsic uncertainties and requires a priori knowledge of the shape distributions (e.g. Min et al., 2004). The retrievals are compared over both ocean and land.

The structure of this paper is as follows: the underlying datasets and retrieval methods used for the evaluation and calibration differences between MODIS and SEVIRI are introduced in Section 2. In Section 3, the across-sensor evaluation design is introduced and the results of the evaluation study are presented and discussed using scenes over both the Atlantic and Central Europe. A summary and final conclusion can be found in Section 4.

Table 1
Spatial and spectral characteristics of the retrievals.

Retrieval	Non-absorbing channel (μm)	Absorbing channel (μm)	Res. Nadir (km)
SLALOM	0.64 over land and 0.81 over ocean	1.64	3×3
M06	0.65 over land and 0.86 over ocean	1.6	1×1
2B-TAU	0.86	2.13	2.5×1.4

2. Data and methods

2.1. Satellite systems used within this study

2.1.1. SEVIRI

For this study, data of MSG SEVIRI, MODIS and CloudSat have been used. The Spinning-Enhanced Visible and Infrared Imager (SEVIRI) on board Meteosat Second Generation (MSG) is the present European geostationary satellite system operated by EUMETSAT. The first satellite of the second generation MSG-1 (Meteosat-8) was launched on 28 August 2002 and is currently positioned at an altitude of about 36,000 km above the equator at 3.4° W. In December 2005, MSG-2 (Meteosat-9) was launched and positioned at 0° longitude (see Munro et al., 2002; Schmetz et al., 2002; Schumann et al., 2002). EUMETSAT and ESA are currently working on Meteosat Third Generation as the follow up mission which is intended to be launched in 2015 (Bézy et al., 2005). SEVIRI measures reflected and emitted radiance in 12 channels, three channels at visible and very near infrared wavelengths (between 0.6 and 1.6 μm), eight at mid-infrared to thermal infrared wavelengths (between 3.8 and 14 μm), and one high-resolution visible channel. SEVIRI scans the full disk every 15 min and provides a nominal spatial

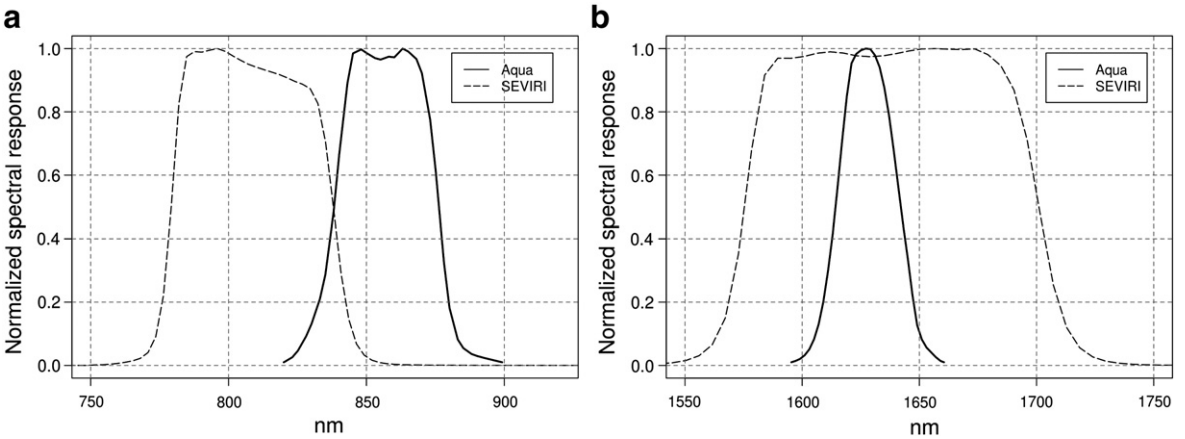

Fig. 2. Spectral response functions of the (a) 0.8 μm and (b) 1.6 μm channels from Aqua MODIS and MSG SEVIRI.

Table 2
Geographic coordinates and satellite zenith angles of the study regions.

Region	Minimum latitude	Maximum latitude	Minimum longitude	Maximum longitude	Minimum satellite zenith	Maximum satellite zenith
North Atlantic	31.00	48.50	−22.50	−12.00	37.70	68.94
Central Europe	40.00	56.00	0.50	18.50	47.30	61.34

resolution of 1 by 1 km at the sub-satellite point for the high resolution channel, and 3 by 3 km for the other channels (Aminou, 2002; Schmetz et al., 2002). Over our study area in Central Europe, the satellite viewing angles of SEVIRI range from 48° to 61° and increase to a range from 38° to 68° over the North Atlantic. As a consequence the above mentioned spatial resolution is reduced in our study. The MSG SEVIRI data required for this study were downloaded from the EUMETSAT data center (www.eumetsat.int) and were pre-processed by the SCISYS Deutschland GmbH (formerly VCS) software package 2met! (http://www.scisys.de/).

2.1.2. MODIS

In addition to MSG SEVIRI, data from the MODerate-resolution Imaging Spectroradiometer (MODIS) on board the Terra and Aqua satellites is used. MODIS measures reflected and emitted radiance in 36 spectral bands ranging from 0.42 to 14.24 μm. Depending on the spectral band the spatial resolution for nadir views range from 250 m to 1 km. Beside the MODIS cloud property product (see below), MODIS geolocation dataset (MODIS 03) and MODIS calibrated radiances with a spatial resolution of 1 km (MODIS 021KM, both available at http://ladsweb.nascom.nasa.gov/) have been used in this study. The latter products provide information about geolocation, solar and satellite angles as well as calibrated radiances for each MODIS tile which is necessary for the application of SLALOM to MODIS.

2.1.3. CloudSat

CloudSat is another EOS satellite which was launched on 28 April 2006 and is orbiting in formation within the A-Train, a satellite constellation of 7 satellites in a sun-synchronous polar orbit with a ground-track repeat of 16 days (Stephens et al., 2002). The main instrument aboard the satellite is the Cloud Profiling Radar (CPR), a 94 GHz nadir-looking radar that measures the energy backscattered by precipitation and clouds as a function of distance from the radar (Im et al., 2006).

2.2. Algorithms used within the study

2.2.1. Semi-analytical approach SLALOM

Nauss and Kokhanovsky (2011) have presented a new cloud property retrieval relying on SimpLe Approximations for cLOudy Media (SLALOM). The forward model is based on approximate solutions of the asymptotic radiative transfer theory (e.g. Germogenova, 1963; King, 1987) and provides increased computation speed since the equations can be efficiently solved during runtime. In order to address the restriction of the technique to weakly absorbing media and

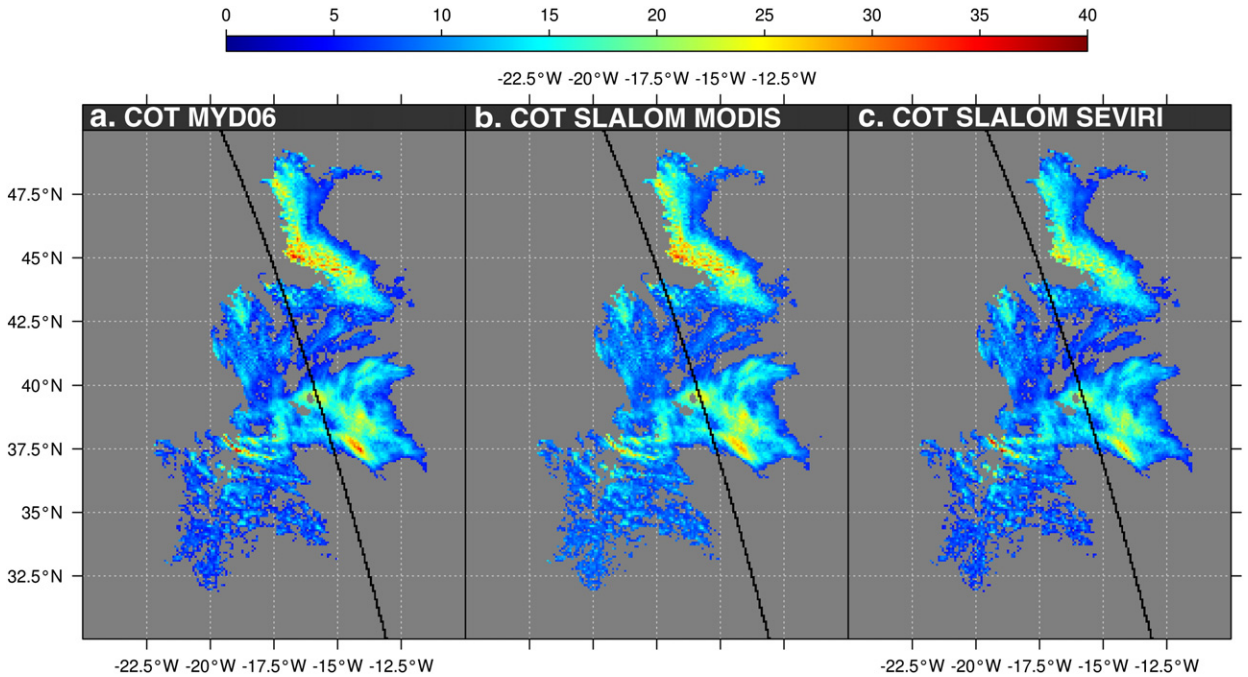

Fig. 3. Cloud optical thickness retrieved by (a) M06, (b) SLALOM using Aqua MODIS data and (c) SLALOM using MSG SEVIRI data for MSG SEVIRI scene from 11 June 2008 14:15 UTC and Aqua MODIS scenes from 11 June 2008 14:15 and 14:20 UTC (values shown for $\tau > 5$; 0.08° to 0.08°). The CloudSat track is denoted by the black line.

small satellite zenith angles, look-up tables for the reflection function of a semi-infinite cloud, the escape function and the spherical albedo are incorporated into the algorithm (see Nauss and Kokhanovsky, 2006 for details). The present version of SLALOM is limited to water clouds.

A detailed description of the algorithm can be found in Nauss and Kokhanovsky (2011) and – in contrast to the website mentioned in that publication – the Fortran source code of the techniques as well as all necessary ancillary datasets have been moved to http://code.google.com/p/rtm-cloud-slalom/ for free download (please do not hesitate to contact the author for assistance).

In order to retrieve cloud optical thickness (τ) and cloud effective droplet radius (a_{ef}) from MSG SEVIRI data, a combination of reflectance measurements at visible (0.65 μm or 0.81 μm) and near-infrared (1.64 μm) wavelengths is used. Necessary look-up tables (see above) have been generated for a droplet size of 10 μm using the radiative transfer code from Mishchenko et al. (1999) in analogy to Nauss and Kokhanovsky (2011). For the background albedo, a minimum composite of the reflectances in the visible (0.65 μm and 0.81 μm) and near-infrared (1.64 μm) channel over one month was calculated. Cloud phase as well as cloud masks were derived using the algorithm developed and implemented by Cermak (2006) and Cermak and Bendix (2008). Besides its application to MSG SEVIRI, SLALOM has also been applied to MODIS data within this study.

Table 3
Comparison of SLALOM and M06 for scenes from Figs. 5 and 6. Columns 1 and 2 are based on the 0.01°×0.01° projection used for the MODIS only comparison while all other columns represent the 0.08°×0.08° resolution of the common evaluation grid between MODIS and MSG SEVIRI. Results are presented for values with $\tau>5/\tau>10$ (Std = standard deviation, Std_Diff = standard deviation of differences, MBE = mean bias error).

	SLALOM MODIS $\tau>5/\tau>10$ 0.01°×0.01°	M06 MODIS $\tau>5/\tau>10$ 0.01°×0.01°	SLALOM SEVIRI $\tau>5/\tau>10$ 0.08°×0.08°	M06 MODIS $\tau>5/\tau>10$ 0.08°×0.08°
Optical thickness				
Min	5.00/10.00	5.00/10.00	5.00/10.00	5.00/10.00
Max	39.68/39.68	40.63/40.63	38.97/38.97	47.00/47.00
Median	10.20/14.70	9.77/14.20	9.43/13.52	9.61/14.59
Mean	11.74/16.04	11.30/15.59	10.45/14.41	11.04/15.72
Std	5.42/4.84	5.41/4.86	4.21/3.56	5.06/4.51
r vs. M06	0.99/0.99		0.95/0.89	
MBE	−0.44/−0.46		0.59/1.31	
Std_Diff	0.51/0.44		5.07/2.08	
Effective radius				
Min	3.00/3.173	1.18/2.49	3.03/5.53	4.95/5.36
Max	37.96/36.74	30.1/29.45	34.51/20.16	19.57/17.75
Median	7.57/8.12	7.32/8.03	7.66/8.24	7.45/7.93
Mean	8.12/8.58	8.07/8.47	8.07/8.68	8.04/8.56
Std	2.88/2.49	2.68/2.36	1.90/1.90	2.00/2.08
r vs. M06	0.94/0.98		0.83/0.91	
MBE	−0.05/−0.10		−0.02/−0.10	
Std_Diff	0.94/0.54		1.17/0.86	

2.2.2. NASA MODIS 06 cloud product

The first retrieval used for the comparison study was developed in the framework of NASA's Earth Observing System (EOS, King and Greenstone, 1999) and is part of the MODIS product. The LUT-based approach (King et al., 1997; Platnick et al., 2003) also uses a combination of one visible and one near-infrared channel to retrieve the aforementioned cloud properties but in order to minimize the influence of the

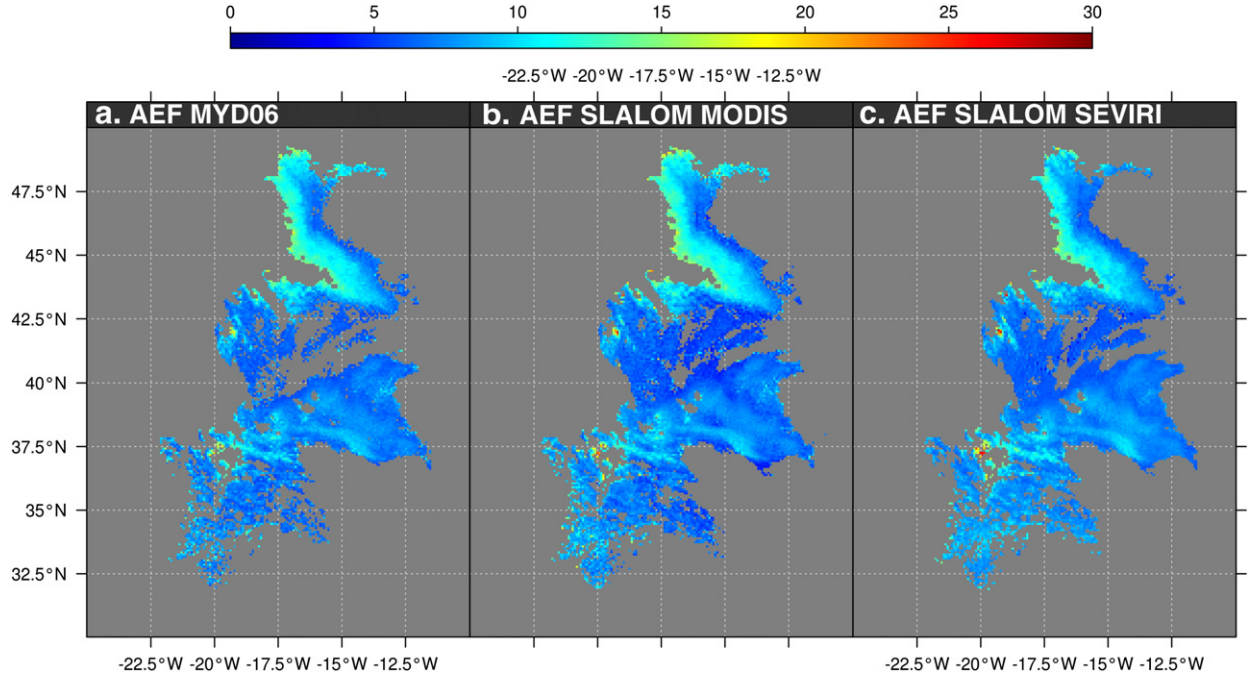

Fig. 4. Cloud effective radius retrieved by (a) M06, (b) SLALOM using Aqua MODIS and (c) SLALOM using MSG SEVIRI data for MSG SEVIRI scene from 11 June 2008 14:15 UTC and for Aqua MODIS scenes from 11 June 2008 14:15 and 14:20 UTC (values shown for $\tau>5$; 0.08°×0.08°).

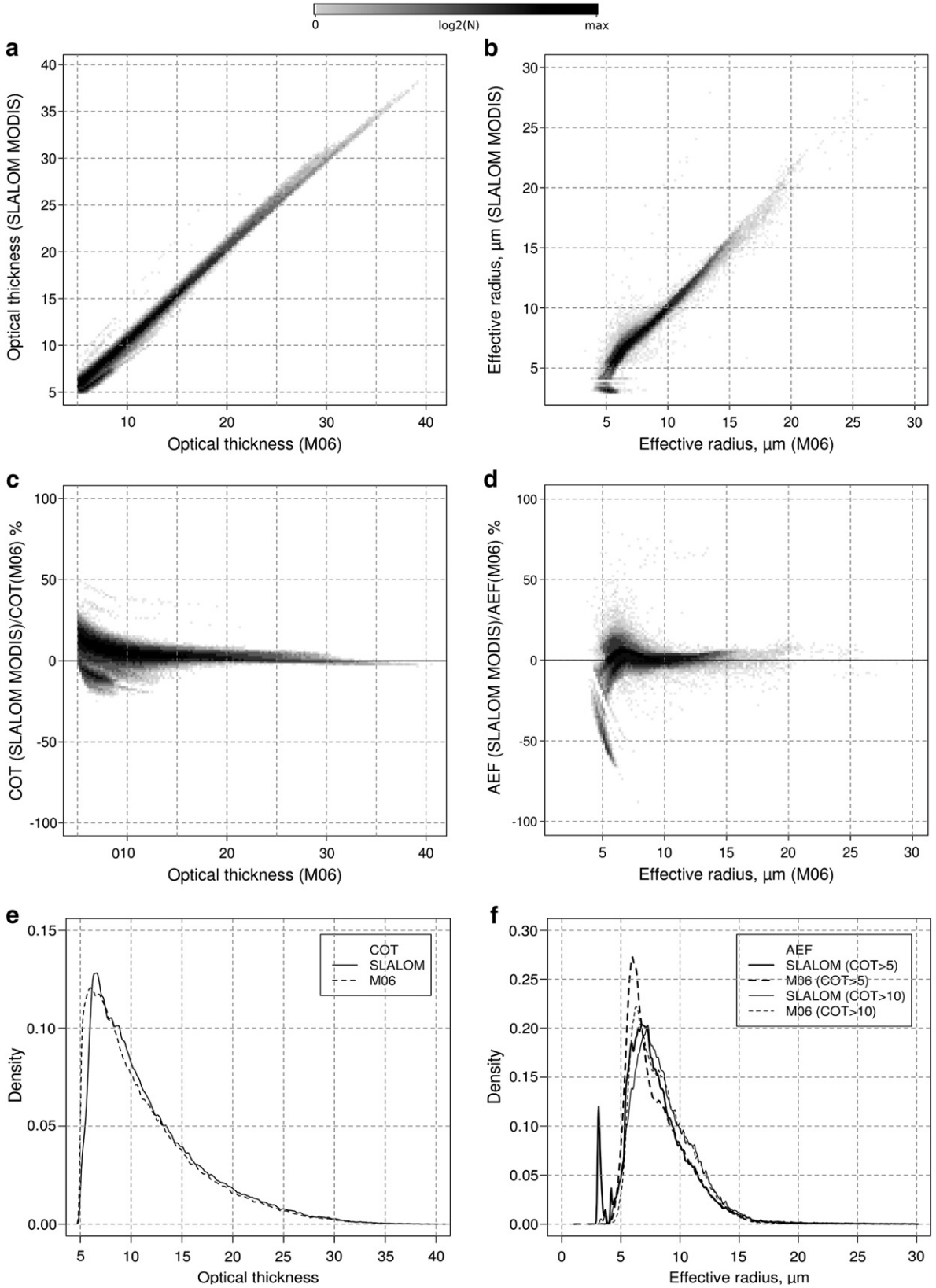

Fig. 5. (a) Cloud optical thickness and (b) cloud effective radius retrieved by SLALOM using MODIS data vs. M06, (c, d) corresponding percentage difference and (e, f) distributions for Aqua MODIS scenes from 11 June 2008, 14:15 and 14:20 UTC (values shown for $\tau > 5$; $0.01° \times 0.01°$).

background reflection, channel 1 (0.65 μm), 2 (0.86 μm) and 3 (1.2 μm) are used over land, ocean, and ice respectively. For the near-infrared, the retrieval is computed for each of channels 6 (1.6 μm), 7 (2.1 μm) and 20 (3.7 μm). The MODIS 06 product (MYD06 for Aqua MODIS and MOD06 for Terra MODIS, both further referred as M06) has a spatial resolution of 1 km and is readily available for download through NASA's Level 1 and Atmosphere Archive and Distribution System (LAADS web, http://ladsweb.nascom.nasa.gov/).

2.2.3. NASA CloudSat 2B-Tau product

Of interest for this study is the 2B-TAU (Cloud optical depth — off nadir) product (Polonsky et al., 2008). Therefore, the 1B-CPR standard product (radar backscatter profiles) is combined with auxiliary MODIS and ECMWF (European Center for Medium-Range Weather Forecasts) data, as well as the 2B-GEOPROF (Cloud geometric profile), 2B-CLDCLASS (Cloud Classification) and CWC-RO (Radar only combined water content) product to produce the 2B-TAU product within a 2.5 km along-track and 1.4 km cross-track radar footprint with 500 m vertical resolution. The sample rate is 0.16 s per profile (Im et al., 2006; Polonsky et al., 2008).

The product contains the total optical depth for each CloudSat profile. The latter is used in this study, because the radar reflectivity measured by the CPR provides detailed information about the cloud in the atmospheric column and serves therefore as a quantitative basis to produce an accurate cloud optical depth profile. Caused by the differing horizontal measurement characteristics of CloudSat and SEVIRI, more than one CloudSat profile is generally located within one SEVIRI pixel, providing an insight into the within-pixel horizontal heterogeneity of the respective area sector. To retrieve the cloud parameters of interest for our study, the day time algorithm uses the upwelling reflectivity at the top of the atmosphere (TOA) measured by MODIS channels 2 (0.864 μm) and 7 (2.13 μm), averaged over an associated subset of 3×5 MODIS pixels (Polonsky et al., 2008). For details on the CloudSat mission, CPR and its products, the reader is referred to http://cloudsat.atmos.colostate.edu and Stephens et al. (2002). As with M06, the 2B-TAU product is already computed and provided by CloudSat Data Processing Center (http://www.cloudsat.cira.colostate.edu/).

2.3. Pre-processing of the MODIS and SEVIRI datasets

In order to compare the retrieved cloud properties based on spatially and temporally corresponding MSG SEVIRI and Terra/Aqua MODIS scenes, both datasets have to be re-projected to a common map projection. In a first step, the MODIS datasets were transformed from their initial HDF-EOS swath format to a geographic projection grid using the Reprojection Tool Swath (see https://lpdaac.usgs.gov/tools/modis_reprojection_tool_swath) with a target resolution of 0.01° by 0.01°. This grid forms the basis for the comparison between the NASA MODIS 06 product and the MODIS-based SLALOM results (for details please refer to the evaluation design presented in Section 3.1). For the evaluation of the SEVIRI-based SLALOM results, the MODIS 06 product as well as the MODIS-based SLALOM results was subsequently averaged to a 0.08° by 0.08° grid. The SEVIRI-reflectances were corrected for sensor ageing (see Section 2.4) and also projected to this geometry. The impact of the different grid resolutions can clearly be seen in Fig. 1. Broken cloud fields which can be recognized in the center of the MODIS image are displayed as rather homogeneous cloud fields in the SEVIRI image.

2.4. Adjustment of SEVIRI reflectances due to sensor ageing and operational calibration uncertainties

Differences in the reflectance measurements will have a direct impact on the retrieved cloud properties since reflection in the VIS is mainly proportional to the cloud optical thickness and reflection in the NIR is mainly inversely proportional to the cloud effective droplet radius. Hence, cross-calibration between different satellite systems is a crucial aspect for long-term and multi-source observations. The MODIS instrument has onboard calibration for all channels and is well-calibrated with an accuracy about 2% (Guenther et al., 1998). The solar channels are calibrated using an onboard solar diffuser, lunar observations and a solar diffuser stability monitor for tracking the solar diffuser degradation. In contrast, there is no onboard calibration device for the solar channels of the SEVIRI instrument. In order to remedy the problem of degradation, the post-launch calibration is done by vicarious calibration techniques. The accuracy of the calibration of the VIS and NIR channels is expected to be about 5%, when adequate data and calibration targets are used (Govaerts and Clerici, 2004). Additionally it should be noted that the corresponding channels have slightly different response functions which also leads to differences in the measured reflectances of SEVIRI and MODIS. As can be seen in Fig. 2a, the response functions for the utilized VIS channel are centered at 0.81 μm (SEVIRI) and 0.86 μm (Aqua MODIS) and have different bandwidths and shapes. Both response functions for the NIR are centered around 1.64 μm, but the SEVIRI bandwidth is almost three times wider than the respective Aqua MODIS channel and their shapes also differ (Fig. 2b).

As a consequence of the calibration procedures and the sensor characteristics, radiances registered by the two sensors differ and effects like sensor ageing will additionally deflect the respective measurements.

Using MODIS as the calibration source, Jan Fokke Meirink (KNMI) has already investigated simultaneous nadir overpasses of MODIS and MSG SEVIRI and found that the calibration of SEVIRI seems to be too dark for VIS and slightly too bright for NIR channels (Meirink, personal communication). He compared Aqua- and Terra MODIS granules near 0°N and 0°E with temporally corresponding SEVIRI images with a maximum time-difference of ±7 min. The results show that the slope between MODIS and SEVIRI is 1.08 for the 0.64 μm channel, 1.06 for the 0.81 μm channel and 0.96 for the 1.64 μm channel. The slopes for Terra MODIS differ by ~1% (Meirink, personal communication). For the present study, these slopes have been applied to the initially received SEVIRI reflectances in order to correct the sensor ageing and calibration deficiencies. However, caused by different viewing conditions (SEVIRI has much larger viewing angles than MODIS) in our study area and the different underlying spatial resolutions and spectral sensor characteristics (e.g. bandwidth, spectral response function) deviations between SEVIRI and MODIS reflectances can be expected, even though the initially received SEVIRI reflectances have been adjusted using the coefficients.

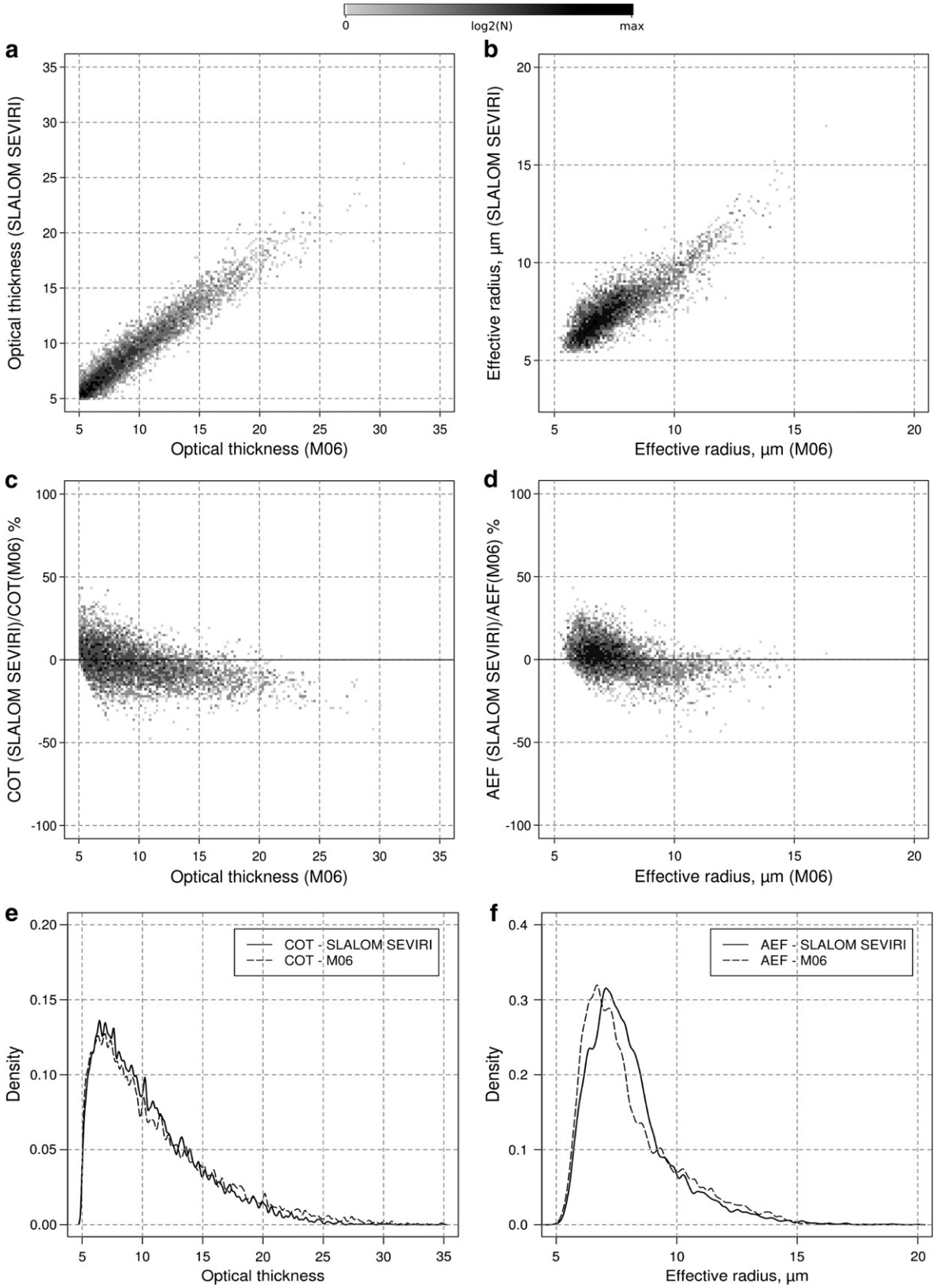

Fig. 6. (a) Cloud optical thickness and (b) cloud effective radius retrieved by SLALOM using MSG SEVIRI data vs. M06, (c, d) corresponding percentage difference and (e, f) distributions for scenes from Figs. 3 and 4 (values shown for $\tau > 5$; 0.08° to 0.08°).

3. Validation of SLALOM retrievals for MODIS and SEVIRI

3.1. Methodology

Since many different cloud property retrievals are used in national and international research projects, it is important to examine possible differences between them. Therefore, SLALOM is compared to well-known and validated retrieval products. The intention is to get information about the relative accuracy between SLALOM and the other retrievals rather than the absolute accuracy against idealized model data (for this topic see Nauss and Kokhanovsky, 2006, 2011). Therefore, the following retrieval-sensor combinations will be evaluated against each other in a three-step approach:

- First, SLALOM will be applied to Terra/Aqua MODIS data and the results will be compared against the NASA MODIS M06 product on a 0.01° by 0.01° grid (King et al., 1997; Platnick et al., 2003).
- Second, SLALOM will be applied to MSG SEVIRI data and compared to the NASA MODIS M06 product on a 0.08° by 0.08° grid.
- Third, SLALOM-based cloud optical thickness retrieved from MSG SEVIRI and Aqua MODIS data as well as MODIS M06 cloud optical thickness will be compared to the CloudSat 2B-TAU product (Polonsky et al., 2008).

The first step allows a comparison between two algorithms applied to the same sensor. Hence, differences between SLALOM and the MODIS 06 product can be solely attributed to different assumptions within the retrievals and meta-datasets (e.g. background albedo). In contrast, the second step will also imply potential deviations due to quite different sensor characteristics and viewing geometries which is the reason why the MODIS-based SLALOM results are also incorporated in the comparison of the SEVIRI-based SLALOM results. For the evaluation, one scene over the North Atlantic and some over the European continent will be used. While for the North Atlantic scene the influence of auxiliary data is minimized due to a quite homogeneous ocean background albedo, the comparison over Central Europe exhibits a considerably higher influence on the resulting parameters of both background albedo and larger satellite viewing angles.

Table 1 shows the absorbing and non-absorbing channels which are used to retrieve cloud optical thickness and effective radius by the different optical algorithms. Since the 1.6 μm channel of SEVIRI is used to retrieve a_{ef}, the analogous M06 product (see Section 2.2.2) is used for the comparison of a_{ef} to eliminate errors due to different wavelength-dependent penetration depths of the absorbing channels at 1.64 and 2.13 μm into the clouds (see Platnick, 2000).

Since CloudSat provide an accurate cloud optical depth profile and detailed information on the sub-pixel heterogeneity of the cloud structure within the SEVIRI pixel, the CloudSat 2B-TAU ($\tau_{2B\text{-}TAU}$) product was included into the investigation as well. For the comparison of the three types of cloud optical thickness (SLALOM retrieval for MSG SEVIRI ($\tau_{Sslalom}$), SLALOM retrieval for MODIS ($\tau_{Mslalom}$), MODIS M06 (τ_{M06})) to $\tau_{2B\text{-}TAU}$, only those SEVIRI/MODIS pixels which are spatially and temporally co-located to the Nadir scan line of CloudSat can be taken into account. Caused by their differing horizontal pixel dimensions (see chapter 2.1.1 and 2.1.3), more than one CloudSat profile is generally located within one SEVIRI pixel for any given date. Several studies have shown that validation uncertainties can be reduced by using a series of corresponding measurements instead of using only the nearest neighbour (e.g. Greuell and Roebeling, 2009; Schutgens and Roebeling, 2009). Therefore, to remedy the scale differences, a mean over all CloudSat optical depth profiles within each SEVIRI pixel is calculated for the comparison. In order to get information about the sub-pixel heterogeneity of the cloud structure, the value range of the individual profiles is discussed.

Due to the complexity of light transport through highly inhomogeneous crystalline clouds, retrievals for ice clouds are generally less accurate (Min et al., 2004). Therefore, only the case of liquid clouds is considered here and water clouds have been selected using the algorithm developed and implemented by Cermak (2006) and Cermak and Bendix (2008). Furthermore, pixels immediately located along the border of clouds are eliminated since sub-pixel cloudiness and enhanced 3-D effects can lead to significant and algorithm-dependent errors in the retrieved cloud property values. With respect to pixels that are affected by the rainbow and the glory, SEVIRI pixels with scattering angles between 134° and 140° and close to 180° were excluded. Reflectance at these angles is more influenced by the shape of the size distribution and not only by the effective radius. Finally, since a number of 1.6-μm detectors on the Aqua MODIS instrument are inoperative (Platnick et al., 2009) those pixels are eliminated within this study as well.

3.2. Results

3.2.1. Results over the North Atlantic

For the comparison over the ocean, the MSG SEVIRI scene from 11 June 2008 at 14:15 UTC (Fig. 1b) and the spatially and temporally co-located Aqua MODIS scenes from 11 June 2008, 14:15 and 14:20 UTC were chosen (Fig. 1a). The area covers the Atlantic Ocean adjacent to the west coast of Europe (geographic boundaries are listed in Table 2) and clouds are located completely over the ocean. Thus, the influence of the background reflection is minimized. The MSG viewing angles range from about 38° to 68°.

To evaluate the performance of SLALOM while minimizing the aforementioned potential error sources that depend on the satellite characteristics, i.e. different viewing geometries, instrument calibration and spectral resolution, a comparison between SLALOM applied to Aqua MODIS data and the NASA MODIS M06 product is carried out first. Hence, differences can be solely attributed to different assumptions within the retrievals and potentially negligible background albedo. Optical thickness (effective radius) of the chosen cloud field can be seen in Fig. 3a and b (Fig. 4a and b). Please note that in these figures, the scenes have already been projected to the grid used for the SEVIRI/MODIS comparison but the statistics have been computed using the 0.01° by 0.01° grid. By using only pixels with an optical thickness larger than 5 in both retrievals, a test sample of 369,185 pixels is used for this first comparison. A statistical summary is presented in the first two columns of Table 3.

Values for the optical thickness of SLALOM and M06 range from 5 to about 40 with very similar mean values of 11.74 (SLALOM) and 11.30 (M06) and standard deviations of 5.42 (SLALOM) and 5.41 (M06) respectively and the two datasets

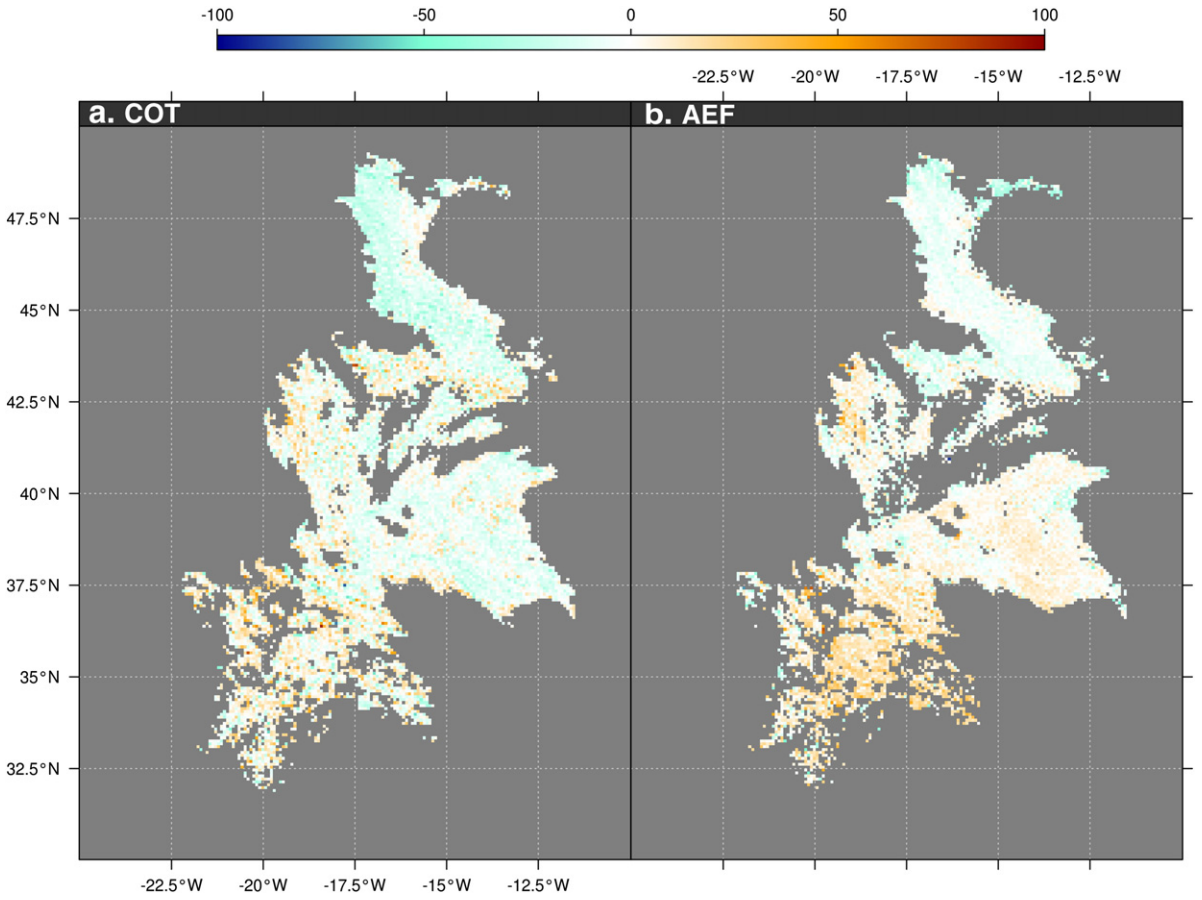

Fig. 7. Spatial distribution of the percentage deviation of (a) cloud optical thickness and (b) cloud effective radius retrieved by SLALOM and M06 for scenes from Figs. 3a and c and 4a and c (values shown for $\tau > 5$; $0.08° \times 0.08°$).

show a strong linear correlation with a coefficient of correlation r of 0.99 (see Fig. 5a). The corresponding percentage difference is shown in Fig. 5c. For τ smaller than 12, the SLALOM values are predominantly larger than the M06 values and the variations range between −20% and +25% with maximum deviations for some pixels as high as 50%. With increasing τ, the spread decreases and the deviation stays mainly between −2% and +10%.

The corresponding effective radius retrievals show similar correlation with r of 0.94 (Fig. 5b). Again, the deviation decreases toward larger a_{ef}. The rather strong deviations of more than −50% for a_{ef} values around 4 are linked to clouds with small optical thickness ($\tau < 10$) and are based on pixels located toward the cloud borders. The coefficient of

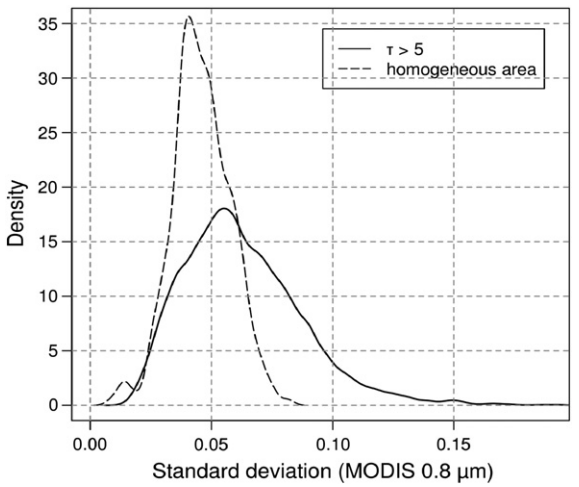

Fig. 8. Distributions of standard deviations arose from MODIS 0.8 µm reflectances lying within one MSG SEVIRI pixel.

Table 4
Statistical values from the dataset of spatially and temporally corresponding $\tau_{Mslalom}$, τ_{M06} and $\tau_{2B\text{-}TAU}$ for scenes from Fig. 5a and b.

Optical thickness	SLALOM MODIS	M06 MODIS	2B-TAU CloudSat
Min	5.28	5.24	1.01
Max	29.27	28.28	31.79
Median	10.89	10.36	10.82
Mean	12.64	12.2	12.92
Std	5.67	5.52	6.28
r vs. 2B-TAU	0.95	0.96	
MBE	0.28	0.72	
Std_Diff	1.98	1.98	

Table 5
Statistical values from the dataset of spatially and temporally corresponding $\tau_{Sslalom}$ and $\tau_{2B\text{-}TAU}$ for scene from Fig. 5c (mean over all CloudSat profiles located within one SEVIRI pixel is taken).

Optical thickness	SLALOM MSG SEVIRI	2B-TAU CloudSat
Min	3.06	0.55
Max	25.33	30.77
Median	10.01	8.97
Mean	10.75	10.36
Std	5.76	6.76
r vs. 2B-TAU	0.92	
MBE	−0.42	
Std_Diff	2.67	

correlation r increases to 0.98, if just a_{ef} values with $\tau > 10$ are considered.

In general, SLALOM and M06 retrieved cloud parameters show only some small differences and the overall agreement is very good. A perfect agreement cannot be expected even between retrievals of the same type (e.g. Nauss et al., 2005). Since both SLALOM and M06 are based on the same MODIS dataset, the results from Fig. 5 and the first two columns of Table 3 can be regarded as a relative baseline for the following evaluations with respect to the interpretation of the agreement between the SEVIRI-, MODIS-, and CloudSat-based results discussed in the next section.

In the second step, SLALOM is applied to MSG SEVIRI data and compared to the MODIS M06 product on the 0.08° by 0.08°

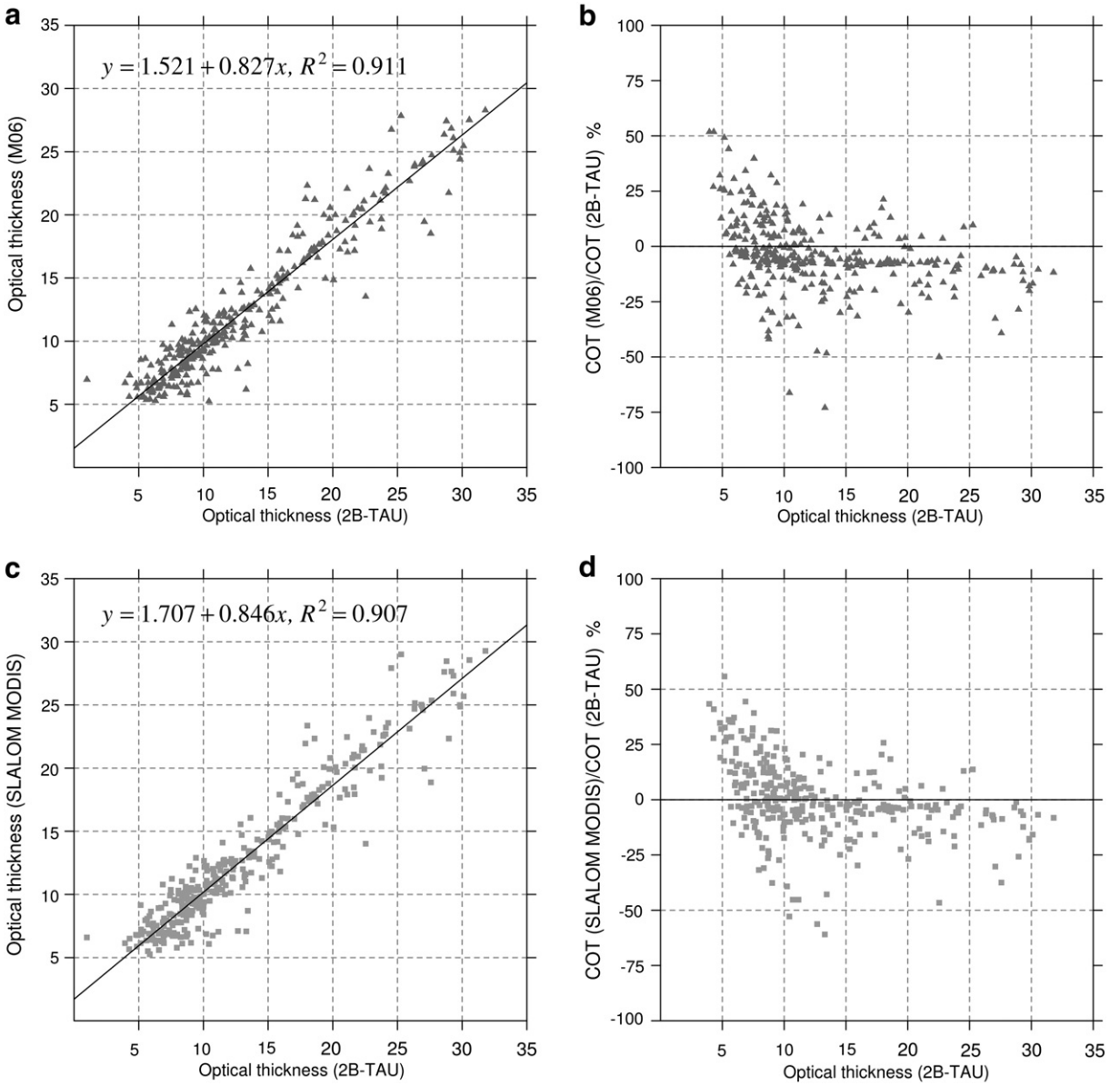

Fig. 9. (a) Cloud optical thickness retrieved by SLALOM using Aqua MODIS data and (c) M06 vs. CloudSat 2B-TAU optical thickness and (b, d) corresponding percentage difference for scenes from Fig. 3a and b.

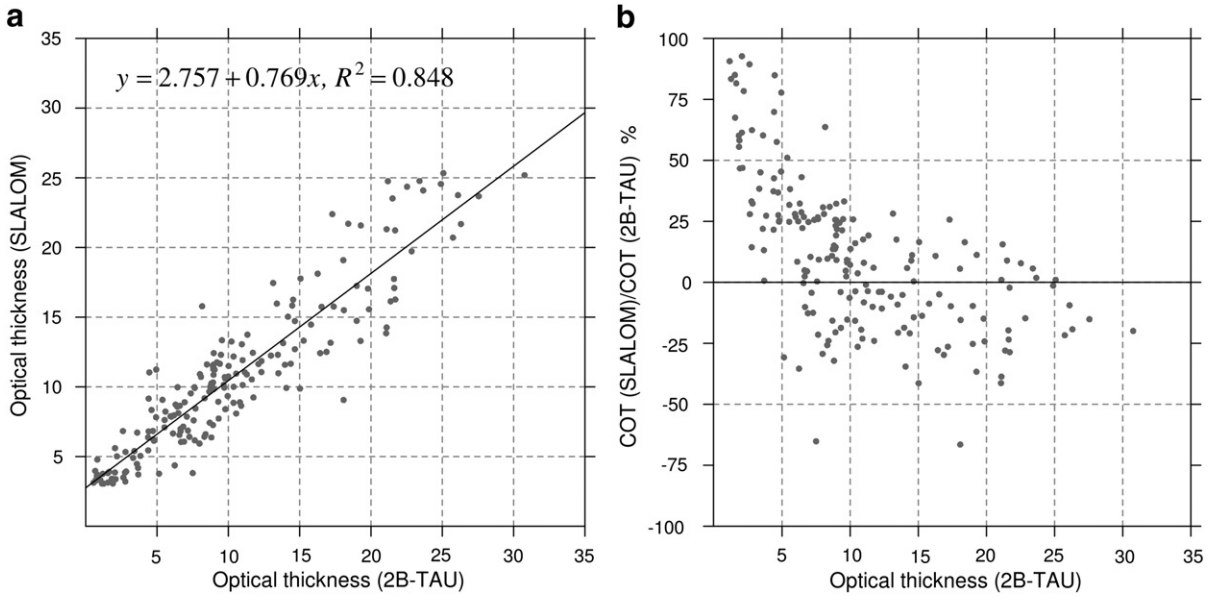

Fig. 10. (a) Cloud optical thickness retrieved by SLALOM using MSG SEVIRI data vs. CloudSat 2B-TAU optical thickness and (b) corresponding percentage difference for North Atlantic scene from 11 June 2008, 14:15 UTC (mean over all CloudSat profiles within one SEVIRI pixel is taken).

grid as well as the CloudSat 2B-TAU product. In contrast to the previous investigation, this comparison implies potential errors arising from issues related to different satellite sensors characteristics.

First, the differences between SLALOM using MSG SEVIRI data and the MODIS M06 product are evaluated. Optical thickness (effective radius) retrieved by SLALOM and M06 are shown in Fig. 3a and c (Fig. 4a and c). Taking into account only values with $\tau > 5$ leads to a test sample of 9348. An overview of the dataset is listed in columns three and four of Table 3. The scatter plots and distributions of $\tau_{Sslalom}$ versus τ_{M06} (Fig. 6a and e) and $a_{efSslalom}$ versus a_{efM06} values (Fig. 6b and f) reveal that the relative number of smaller values is strongly increased in comparison to the results presented in the preceding study. This can probably be attributed to the different viewing geometries of each satellite.

$\tau_{Sslalom}$ and τ_{M06} show a coefficient of correlation r of 0.95 (Fig. 6a) and their distributions have a very similar shape and positive skewness (Fig. 6e). The corresponding percentage difference in Fig. 6c illustrates that for τ smaller than 10, SLALOM values are predominantly larger than the M06 values and the variations range mainly between −10% and +30%.

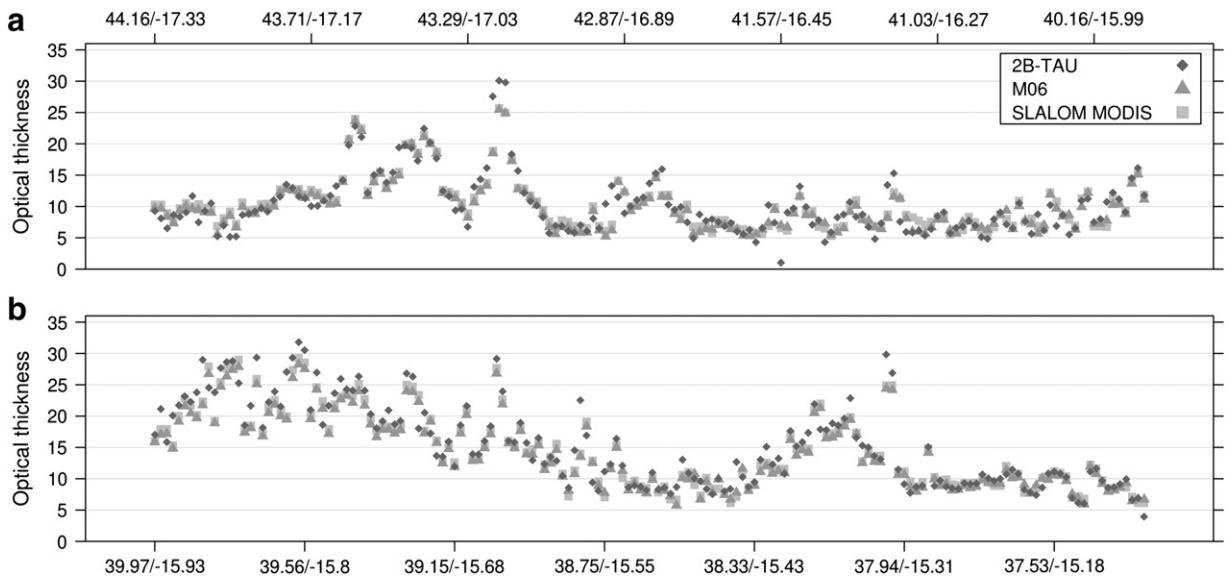

Fig. 11. Cloud optical thickness retrieved by SLALOM using Aqua MODIS data, M06 and CloudSat 2B-TAU optical thickness for scenes from Fig. 3a and b. Retrieved τ values are displayed for each MODIS pixel.

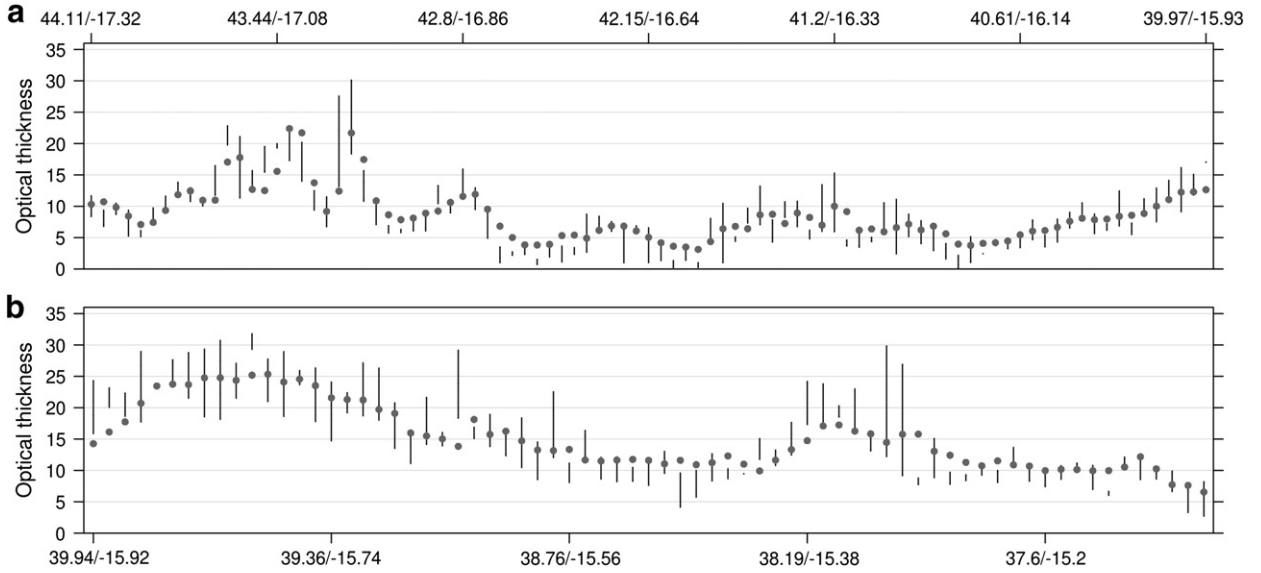

Fig. 12. Cloud optical thickness retrieved by SLALOM using MSG SEVIRI data vs. CloudSat 2B-TAU optical thickness for scene from Fig. 3c. For each SEVIRI pixel the retrieved $\tau_{Sslalom}$ value (grey dot) and the range of spatial corresponding $\tau_{2B\text{-}TAU}$ values (black line) are displayed.

With increasing τ, the spread decreases. The spatial percentage differences shown in Fig. 7a show that higher deviations can mainly be found in the southern, less homogeneous cloud area where the differences can mainly be attributed to the different spatial resolutions of the two sensors and the larger SEVIRI pixels may encompass a mixed cloud scenario. Since all retrievals assume plane-parallel and homogeneous clouds throughout each pixel, this type of error generally increases with pixel size because the area of unknown inhomogeneity within the pixel increases (Zinner et al., 2005). To get information about the cloud horizontal homogeneity for each SEVIRI pixel, the standard deviation of MODIS reflection values of the 0.856 μm channel (0.01° to 0.01°) lying within one SEVIRI pixel is calculated. Fig. 8 shows the distribution of standard deviations considering all SEVIRI pixels within the considered cloud area shown in Fig. 3 with $\tau > 5$ (black line). A high number of SEVIRI pixels encompass non-homogeneous clouds with standard deviations of up to 0.19. The horizontal homogeneous index (i.e. the mean over all standard deviations) is 0.05. For comparison, if only pixels lying within the homogeneous area around 38.5 N° and 14° W are taken into consideration, the relative number of smaller standard deviations is increased and values range to 0.085 (dashed line). The corresponding homogeneous index decreases to 0.046.

The scatter plot of $a_{efSslalom}$ against a_{efM06} in Fig. 6b reveals a correlation with r of 0.83. As can be seen in Fig. 6d, the corresponding percentage difference reveals that $a_{efSslalom}$ are generally larger for $a_{ef} < 9.0$ μm and show deviations of up to about +40% for decreasing a_{ef}. For $a_{ef} > 9.0$ μm $a_{efSslalom}$ values are smaller and deviation ranges generally between +5% and −10%. The deviations of some single pixels are around ±50%. The different modes of the $a_{efSslalom}$ and a_{efM06} distributions shown in Fig. 6f might be caused by the distributions of SLALOM and SEVIRI reflectances at 1.6 μm.

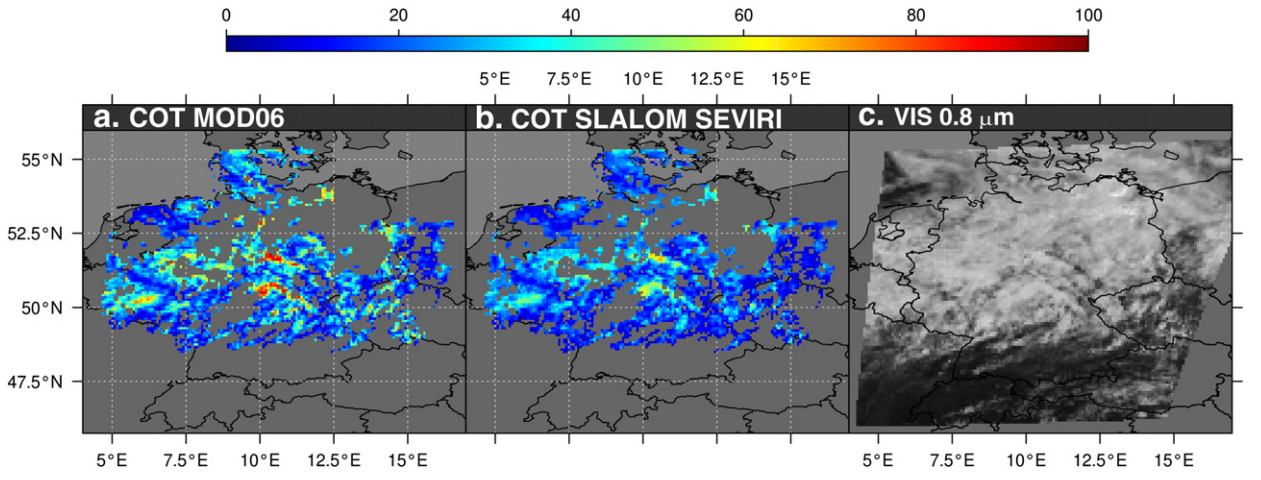

Fig. 13. Cloud optical thickness retrieved by (a) M06, (b) SLALOM using MSG SEVIRI data and (c) reflections of MSG SEVIRI 0.84 μm-channel for MSG SEVIRI scene from 28 June 2008 09:45 UTC and Terra MODIS scene from 28 June 2008 10:00 UTC (values shown for $\tau > 5$; 0.08°×0.08°).

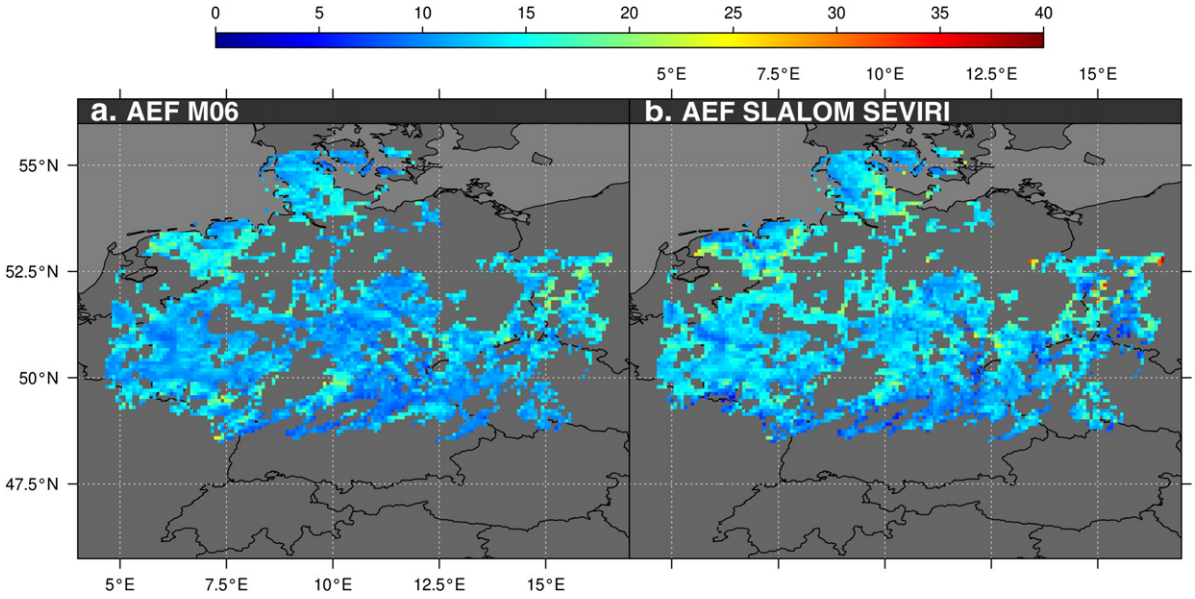

Fig. 14. Cloud effective droplet radius retrieved by (a) SLALOM using MSG SEVIRI data and (b) M06 for MSG SEVIRI scene from 28 June 2008 09:45 UTC and Terra MODIS scene from 28 June 2008 10:00 UTC (values shown for $\tau > 5$; 0.08°×0.08°).

A spatial representation of the relative differences between the two datasets is given in Fig. 7b. The largest deviations with a bias of ±30% and some single pixels up to ±60% can be found mainly in the south-western area and again along the cloud borders. These deviations are likely to be traced back to enhanced 3D effects resulting from horizontally and vertically inhomogeneous clouds and sub-pixel cloudiness often occurring at the cloud edges.

In the third step, the comparison of the three different types of cloud optical thickness $\tau_{Sslalom}$, $\tau_{Mslalom}$ and τ_{M06} against the CloudSat 2B-Tau product is carried out. CloudSat provide an accurate cloud optical depth profile and detailed information on the sub-pixel heterogeneity of the cloud structure within the SEVIRI pixel.

τ_{M06}, $\tau_{Mslalom}$ and $\tau_{Sslalom}$ as well as the CloudSat track are shown in Fig. 3a, b and c, respectively. Datasets of spatially and temporally corresponding pairs of optical thickness derived by M06, $SLALOM_M$, $SLALOM_S$ and CloudSat 2B-TAU are extracted. Taking into account all temporally and spatially corresponding pixels leads to a test sample of 686 ($SLALOM_S$) and 337 ($SLALOM_S$, M06) value pairs. Note that the test sample of MODIS is reduced in comparison to SEVIRI, since a number of 1.6-μm detectors on the Aqua MODIS instrument are inoperative and therefore those pixels are eliminated

Table 6
Comparison of SLALOM and M06 for scenes from Figs. 13 and 14. Columns 1 and 2 are based on the 0.01°×0.01° projection used for the MODIS only comparison while the other columns represent the 0.08°×0.08° resolution of the common evaluation grid between MODIS and MSG SEVIRI. Results are presented for values with $\tau > 5/\tau > 10$.

	SLALOM MODIS $\tau>5/\tau>10$ 0.01°×0.01°	M06 MODIS $\tau>5/\tau>10$ 0.01°×0.01°	SLALOM SEVIRI $\tau>5/\tau>10$ 0.08°×0.08°	M06 MODIS $\tau>5/\tau>10$ 0.08°×0.08°
Optical thickness				
Min	5.00/10.00	5.01/10.02	5.33/10.65	5.03/10.02
Max	98.67/98.67	99.98/99.98	72.81/72.81	97.43/97.44
Median	22.84/26.10	22.94/26.42	18.51/21.45	23.31/27.04
Mean	25.23/28.56	26.98/30.57	20.29/23.59	26.68/30.49
Std	13.16/12.54	16.52/15.89	10.62/9.70	15.52/15.03
r vs. M06	**0.95/0.92**		**0.82/0.80**	
MBE	2.20/2.55		**6.39/6.90**	
Std_Diff	7.15/7.75		**9.10/9.22**	
Effective radius				
Min	3.00/3.10	4.35/4.35	4.55/7.23	6.50/7.30
Max	37.15/37.04	35.05/35.05	36.60/36.60	25.64/25.64
Median	10.53/10.96	11.8/11.7	12.83/13.20	11.85/11.70
Mean	10.84/11.44	12.29/12.13	13.07/13.57	12.30/12.13
Std	3.39/3.10	3.10/2.95	2.93/2.58	2.43/2.27
r vs. M06	0.68/0.89		0.52/0.68	
MBE	1.45/0.68		−0.77/−1.44	
Std_Diff	2.62/1.45		2.68/1.95	

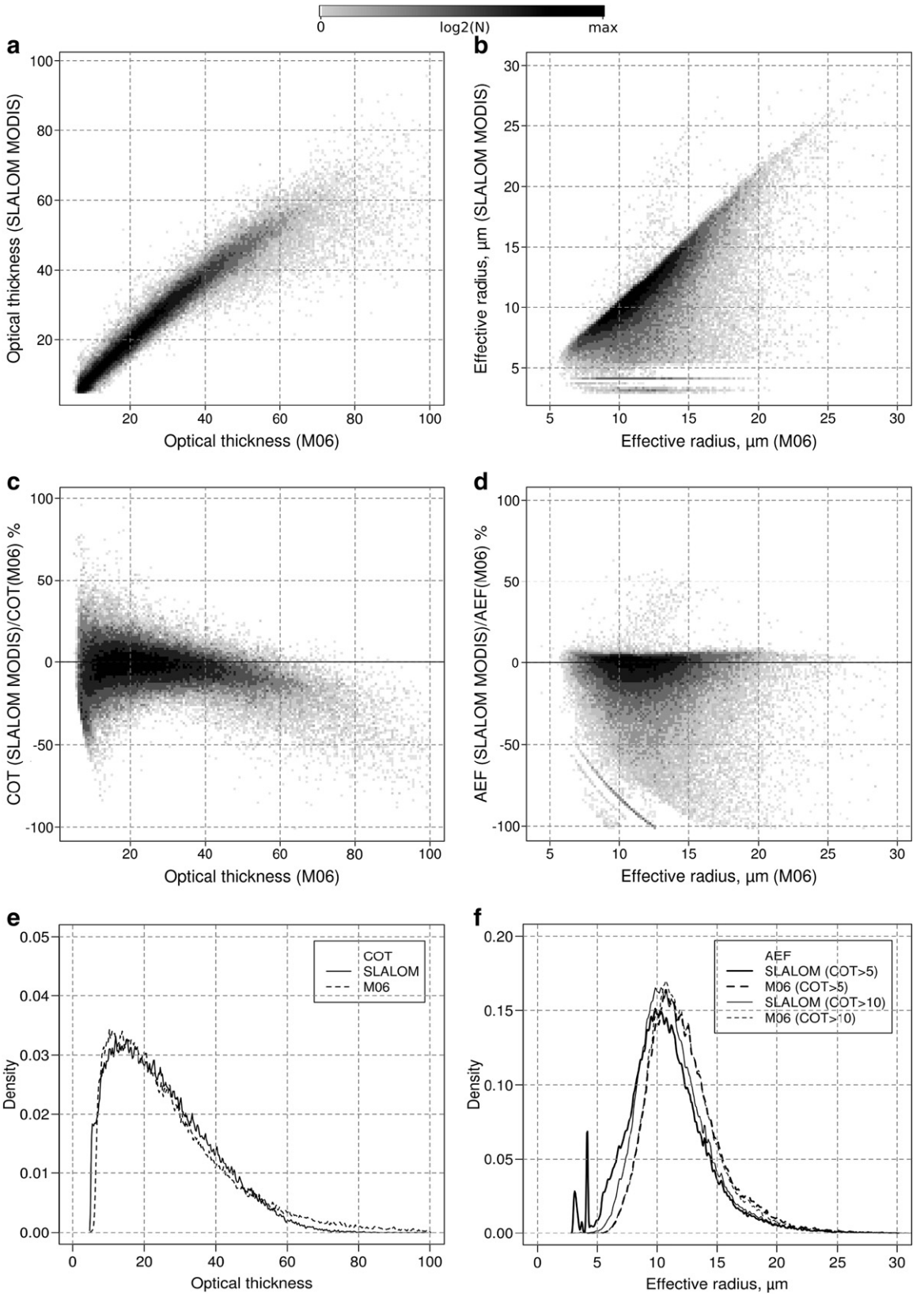

Fig. 15. (a) Cloud optical thickness and (b) cloud effective radius retrieved by SLALOM using MODIS data vs. M06, (c, d) corresponding percentage difference and (e, f) distributions for Terra MODIS scene from 28 June 2008 10:00 UTC (values shown for $\tau > 5$; $0.01° \times 0.01°$).

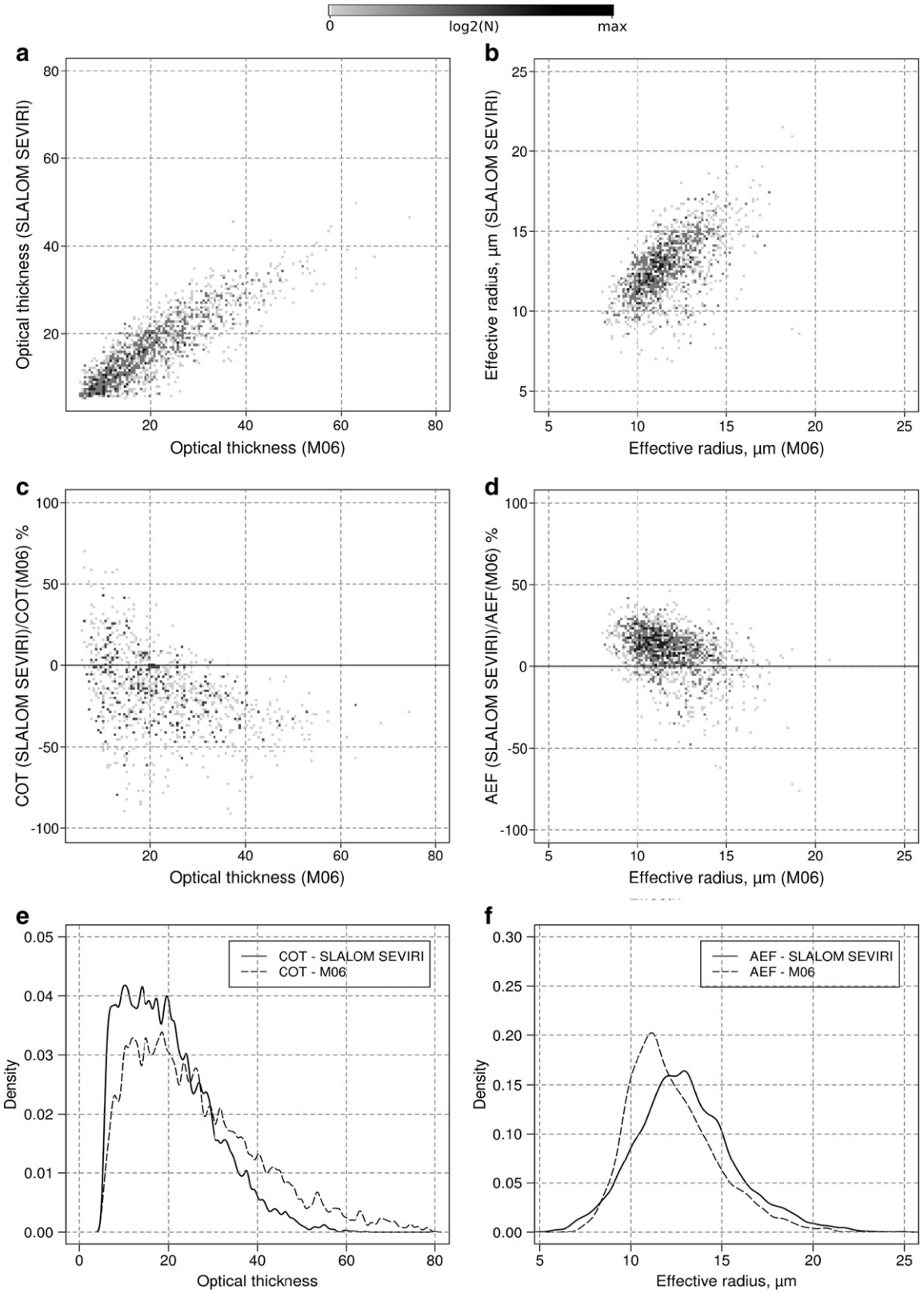

Fig. 16. (a) Cloud optical thickness and (b) cloud effective radius retrieved by SLALOM using MSG SEVIRI data vs. M06, (c, d) corresponding percentage difference and (e, f) distributions for MSG SEVIRI scene from 28 June 2008 09:45 UTC and Terra MODIS scene from 28 June 2008 10:00 UTC (values shown for $\tau > 5$; $0.08° \times 0.08°$).

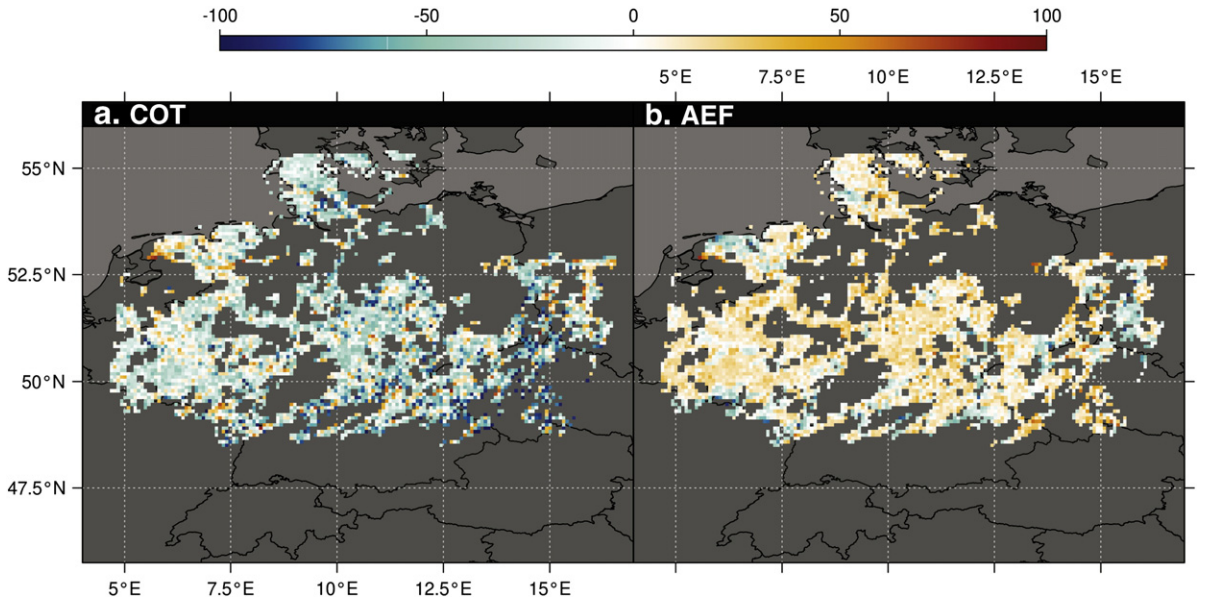

Fig. 17. Spatial distribution of the percentage deviation of (a) cloud optical thickness and (b) cloud effective radius retrieved by SLALOM and M06 for scenes from Fig. 13a and b (optical thickness) and 14a and b (effective radius) (values shown for $\tau > 5$; $0.08° \times 0.08°$).

within this study. Due to their different viewing characteristics, between one and five CloudSat profiles can be found within one MSG SEVIRI pixel. Therefore a mean over all CloudSat profiles located within one MSG SEVIRI pixel is taken for the present evaluation. As a result, the number of test samples is reduced to 175 ($SLALOM_S$). Tables 4 and 5 summarize basic descriptive statistics of the mentioned datasets.

The minimum values of 2B-TAU are lower and the maximum values are higher than those inferred from $SLALOM_M$, M06 and $SLALOM_S$. The latter as well as the higher standard deviations of the 2B-TAU datasets indicate a typical behavior when datasets with higher spatial resolution are compared to datasets with lower resolution. The mean optical thickness of 10.75 ($SLALOM_S$) and 10.36 (2B-TAU) as well as the mean values of 12.64 ($SLALOM_M$), 12.2 (M06) and 12.92 (2B-TAU) are very close to each other. As can be seen in the scatter plots shown in Fig. 9a and c, $\tau_{Mslalom}$ and $\tau_{2B\text{-}TAU}$ as well as τ_{M06} and $\tau_{2B\text{-}TAU}$ reveal a clear positive correlation with coefficients of correlation of 0.95 and 0.96. The corresponding percentage differences of both datasets (Fig. 9b and d) show a very similar spreading. For τ smaller than 10, $\tau_{Sslalom}/\tau_{M06}$ values are larger than the corresponding $\tau_{2B\text{-}TAU}$ values. With increasing τ, the spread decreases and the deviation ranges mainly between −30% and +25%. $\tau_{Sslalom}$ and $\tau_{2B\text{-}TAU}$ possess a slightly smaller but still very good correlation with r of 0.92 (Fig. 10a). The spreading of the corresponding percentage differences (Fig. 10b) is very similar to those shown in Figs. 9b and d.

Figs. 11 and 12 show the evolution of τ_{M06}, $\tau_{Mslalom}$ and $\tau_{Sslalom}$ values in comparison to spatially corresponding $\tau_{2B\text{-}TAU}$ values for each Aqua MODIS/MSG SEVIRI pixel along the tracks depicted in Fig. 3a, b and c from N–S. Hence the first pixel in the upper part of Figs. 11 and 12 corresponds to the northernmost pixel in the satellite images and the following data pairs represent the development along the CloudSat track to the southern part. Fig. 11 indicates that in most cases τ_{M06} and $\tau_{Mslalom}$ values correspond very well with CloudSat 2B-Tau. In contrast to the MODIS-based comparison where only one CloudSat profile can be located within one MODIS pixel, it is possible to locate one to five CloudSat profiles within one MSG SEVIRI pixel. In order to get also information about sub-pixel cloud heterogeneity within one MSG SEVIRI pixel, instead of the mean over all CloudSat profiles assigned to the accordingly pixel, the evolution of $\tau_{Sslalom}$ values (grey dots) in comparison to the range of spatially corresponding $\tau_{2B\text{-}TAU}$ values (black lines) within each MSG SEVIRI pixel is shown in Fig. 12. The results indicate that in most cases $\tau_{Sslalom}$ values are well within the range of corresponding $\tau_{2B\text{-}TAU}$ values except for very small optical thickness (smaller than 5) which are overestimated by SLALOM. Cloud inhomogeneities are evident through large ranges of $\tau_{2B\text{-}TAU}$ values that can be seen within some MSG SEVIRI pixels. Due to the larger MSG SEVIRI pixels, the likelihood of a mixed cloud scenario being located within one pixel is increased, which is likely to result in less accurate estimations of cloud optical thickness in these cloud areas as compared to CloudSat. However, the overall evolution is mapped very well by the $\tau_{Sslalom}$ values.

While this section has been restricted to an evaluation between the SLALOM, M06 and CloudSat 2B-TAU product over ocean, the situation is complicated over land. There, the influence of the ground surface reflection increases and the resulting consequences are presented in the next section.

3.2.2. Results over Central Europe

The MSG SEVIRI scene from 28 June 2008 at 09:45 UTC and the temporally and spatially co-located Terra MODIS scene from 28 June 2008 at 10:00 UTC were chosen for the comparison over land. The area covers Germany according to the geographic boundaries listed in Table 2.

Just like in the previous comparison, SLALOM will be applied to MODIS data and the results will be compared

against the MODIS M06 product first. The results of the analogous comparison of SLALOM against M06 over the ocean are shown in Fig. 5 and the first two columns of Table 3 reveal differences between the algorithms over the ocean and therefore over an area with quite homogeneous background albedo. These results can be regarded as baseline for the following evaluation with respect to the interpretation of the agreement between SEVIRI and MODIS-based results over land where the influence of background albedo strongly increases.

The cloud field which is taken into consideration can be seen in the area of the retrieved optical thickness in Fig. 13a (M06) and b (SLALOM) and the retrieved effective radius in Fig. 14a (M06) and b (SLALOM) (please note again, that these images have been reprojected to the 0.08° to 0.08° grid used for the SEVIRI/MODIS comparison but the statistical evaluation has been performed on the initial 0.01° grid). Ice phase clusters within the cloud fields are excluded from the comparison and once again, only clouds with $\tau > 5$ are taken into account. A statistical overview about the dataset is listed in the first two columns of Table 6.

As can be seen in Fig. 15a, optical thickness values retrieved by SLALOM and M06 show good agreement with r of 0.95. For τ smaller than 20, the SLALOM deviations range mainly between $\pm 20\%$ and with increasing τ, the spread

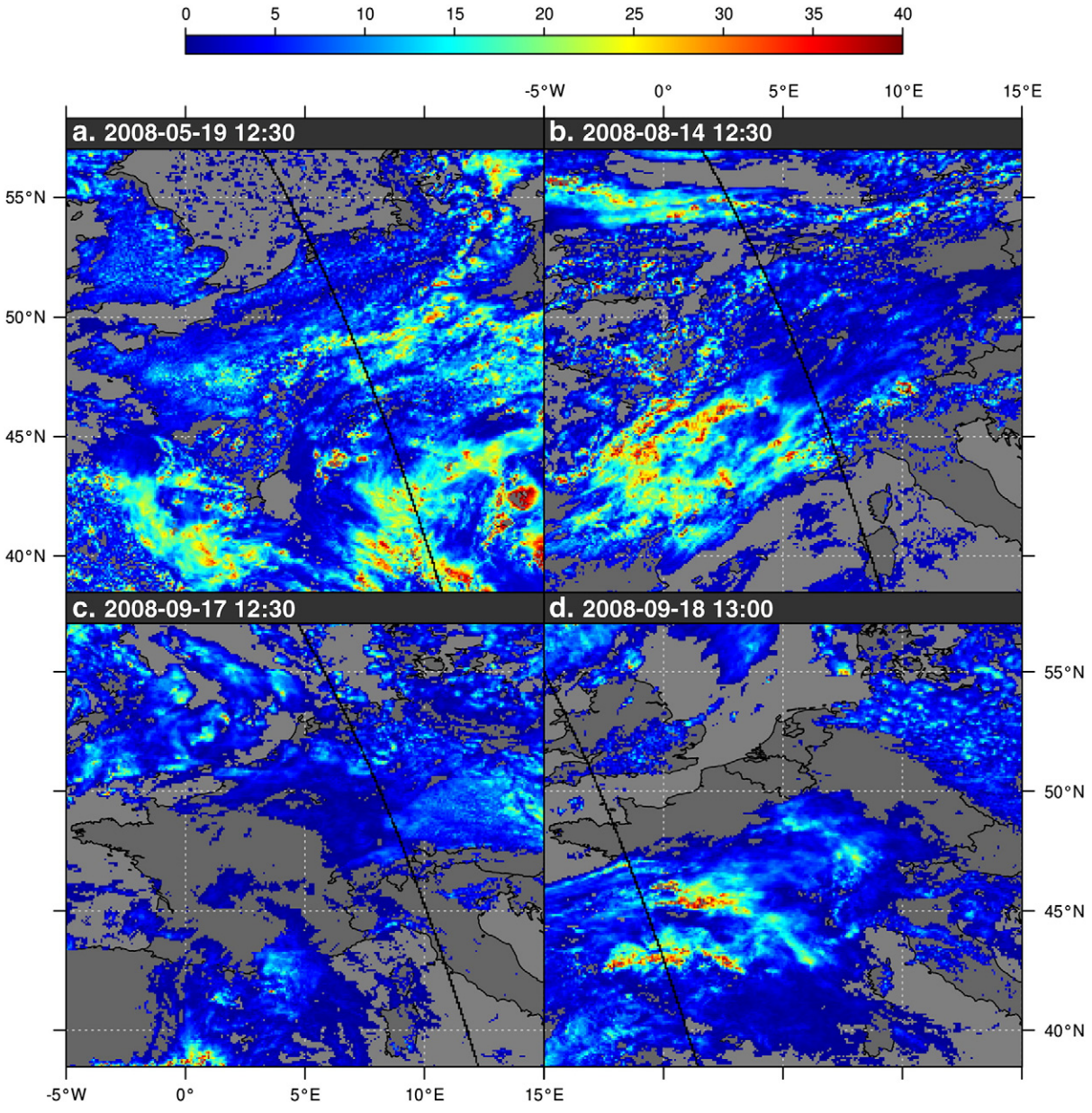

Fig. 18. Cloud optical thickness retrieved by SLALOM for scenes over Europe, (a) May 19th 2008 12:30 UTC, (b) August 14th 2008 12:30 UTC, (c) September 17th 2008 12:30 UTC and (d) September 18th 2008 13:00 UTC. The CloudSat tracks are denoted by black lines.

decreases initially. For τ larger than 50 the spread increases again and the SLALOM values are predominantly smaller than the M06 values (Fig. 15c). Fig. 15e shows that both distributions have a positive skewness and show very good agreement.

The corresponding effective radius shows a correlation coefficient r of 0.64. As can be seen in Fig. 15d, the percentage difference reveal that $a_{efMslalom}$ are generally smaller and for some pixels the deviations increase up to over −100%. Like over the North Atlantic, the deviations for $a_{efMslalom}$ values around 4 are linked to clouds with small optical thickness ($\tau<10$) and are based on pixels located toward the cloud borders. If only pixels with $\tau>10$ are considered, the distribution of $a_{efMslalom}$ values shows no deviations around 4 and the coefficient of correlation r increases to 0.89.

In the following section the investigation of differences in cloud properties retrieved by SLALOM using MSG SEVIRI data compared to M06 is carried out. In contrast to the Atlantic scene, the 0.6 μm channel was used this time to retrieve the SLALOM-based cloud optical properties, since M06 uses the 0.65 μm channel over land surfaces. Figs. 13a and b show the optical thickness retrieved by SLALOM and M06, respectively. The extracted dataset of spatially corresponding $\tau_{Sslalom}$ and τ_{M06} values consists of a test sample of 4452. τ values range from 5 to 97.44 (M06) and 72.81 (SLALOM) (see Table 6 for statistical overview of the dataset). A correlation coefficient of 0.80 reveals a good linear correlation between $\tau_{Sslalom}$ and τ_{M06} (Fig. 16a). The corresponding percentage difference shows that variations range predominantly between −50 and +50% (Fig. 16c).

Retrieved $a_{efSslalom}$ and a_{efM06} values are presented in Fig. 14a and b. The corresponding scatter plot in Fig. 16b and a correlation coefficient r of 0.52 reveal that this correlation is weaker. The main range of a_{ef} values is between 9 and 16 μm and therefore considerably reduced. The values of $a_{efSslalom}$ are mainly larger and show predominantly deviations from −10% to +30% (Fig. 16d). This is also evident in Fig. 17b, where the spatial distribution of percentage difference is shown.

The results of $a_{efSslalom}$ and a_{efM06} show substantially larger differences than the corresponding results for the Atlantic scene, but the overall agreement still indicates a correlation. Other than the aforementioned reasons for the uncertainties (e.g. different retrievals, different satellite systems etc.), the major differences over land result from the influence of the surface albedo and small-scale cloud inhomogeneities. In particular, the larger MSG SEVIRI pixels with a resolution of about 5 to 8 km in the study area are likely to encompass mixed cloud scenarios and gaps in the cloud field which can be described much more precisely by the high resolution MODIS sensor (1 km×1 km).

Just as for the comparison over the Atlantic, the CloudSat 2B-TAU product is included into the investigation. Because of the scattered cloud fields, four scenes from May, August and September 2008 over Central Europe were chosen for the evaluation in order to increase the dataset. Retrieved $\tau_{Sslalom}$ and the corresponding CloudSat tracks are shown for all scenes in Fig. 18. Datasets of spatially and temporally corresponding pairs of optical thickness derived by M06, $SLALOM_M$, $SLALOM_S$ and CloudSat 2B-TAU are extracted. Taking into account all temporally and spatially corresponding pixels leads to a test sample of 1504 ($SLALOM_S$) and 780 ($SLALOM_S$, M06) value pairs. The number of $\tau_{Sslalom}$ test samples is reduced to 409, if a mean over all CloudSat profiles located within one MSG SEVIRI pixel is taken. A summary about the basic descriptive statistics of the mentioned datasets can be found in Tables 7 and 8.

Table 7
Statistical values from the dataset of spatially and temporally corresponding $\tau_{Mslalom}$, τ_{M06} and $\tau_{2B\text{-}TAU}$ for temporally corresponding Aqua MODIS scenes from Fig. 20.

Optical thickness	SLALOM MODIS	M06 MODIS	2B-TAU CloudSat
Min	1.31	1.29	0.10
Max	30.49	72.00	70.21
Median	7.17	9.55	10.15
Mean	8.12	13.08	13.89
Std	5.41	12.51	12.14
r vs. 2B-TAU	0.76	0.81	
MBE	5.76	0.81	
Std_Diff	8.78	7.63	

As can be seen in the scatter plot shown in Fig. 19a, τ_{M06} and $\tau_{2B\text{-}TAU}$ reveal a clear positive correlation with coefficient of correlation of 0.81. The corresponding percentage difference (Fig. 19b) illustrates that for τ smaller than 10, τ_{M06} values show the largest deviations up to −120% to +170%. With increasing τ, the spread decreases and the deviation range mainly between −50% and +50%. The coefficient correlation between $\tau_{Mslalom}$ and $\tau_{2B\text{-}TAU}$ possesses a slightly smaller but still acceptable correlation with r of 0.76 (Fig. 19c). However, as can be seen in Fig. 19d, for τ larger than 10, $\tau_{Mslalom}$ values are always smaller than the corresponding $\tau_{2B\text{-}TAU}$ values. The scatter plot and percentage difference of $\tau_{Sslalom}$ and $\tau_{2B\text{-}TAU}$ (Fig. 20a and b) are very similar to those shown in Fig. 19c and d ($\tau_{Mslalom}$ vs. $\tau_{2B\text{-}TAU}$). $\tau_{Mslalom}$ values are predominantly smaller than the corresponding $\tau_{2B\text{-}TAU}$ values (r = 0.73).

The evolution of τ_{M06}, $\tau_{Mslalom}$ and $\tau_{Sslalom}$ values in comparison to spatially corresponding $\tau_{2B\text{-}TAU}$ values for each Aqua MODIS/MSG SEVIRI pixel along the tracks depicted in Fig. 18 from N–S is shown in Figs. 21 and 22. Fig. 21 indicates that in most cases τ_{M06} values correspond very well with CloudSat 2B-Tau. $\tau_{Mslalom}$ values are generally smaller than the corresponding $\tau_{2B\text{-}TAU}$ values. This is especially pronounced for large $\tau_{2B\text{-}TAU}$ values. In Fig. 22 the evolution of $\tau_{Sslalom}$ values (grey dots) in comparison to the range of spatially corresponding $\tau_{2B\text{-}TAU}$ values (black lines) within each MSG SEVIRI pixel is shown. The large ranges of $\tau_{2B\text{-}TAU}$ values that can be seen within many SEVIRI pixels indicate the presence of significant cloud inhomogeneities. Due to the larger MSG SEVIRI pixels, the likelihood of a mixed cloud scenario being located within

Table 8
Statistical values from the dataset of spatially and temporally corresponding $\tau_{Sslalom}$ and $\tau_{2B\text{-}TAU}$ for scenes from Fig. 20 (mean over all CloudSat profiles located within one SEVIRI pixel is taken).

Optical thickness	SLALOM MSG SEVIRI	2B-TAU CloudSat
Min	0.03	0.10
Max	32.65	101.33
Median	5.80	10.87
Mean	7.87	15.80
Std	6.79	16.10
r vs. 2B-TAU	0.73	
MBE	7.93	
Std_Diff	12.01	

one pixel is increased. The results indicate that the overall evolution is mapped less accurately than the results over the North Atlantic. However, the tendency of the $\tau_{2B\text{-}TAU}$ cloud thickness evolution is mapped very well.

4. Summary and conclusion

The aim of this study was the evaluation of the semi-analytical cloud retrieval algorithm SLALOM ported to SEVIRI on board MSG. The study is motivated by the enhanced information content potentially provided by a temporal high resolution observation system which is especially important if detailed cloud evolution monitoring is necessary or if the cloud properties are subsequently used for the delineation of instantaneously raining from non-raining cloud areas. The evaluation was realized by using two well-known cloud property retrievals, the LUT-based approach by Platnick et al. (2003) and CloudSat 2B-TAU product (Polonsky et al., 2008). The intention was to assess the accuracy of SLALOM using MSG SEVIRI data in real-case situations. To the best of our knowledge it was the first application of SLALOM to geostationary satellite data. For the investigation, two study areas were chosen, one over the North Atlantic where the influence of auxiliary data is minimized (i.e. homogeneous ocean background albedo), and one over Central Europe which exhibits a higher influence of the background albedo and small-scale inhomogeneous clouds. SEVIRI reflectances were recalibrated using calibration coefficients found by Jan Fokke Meirink (KNMI) in order to

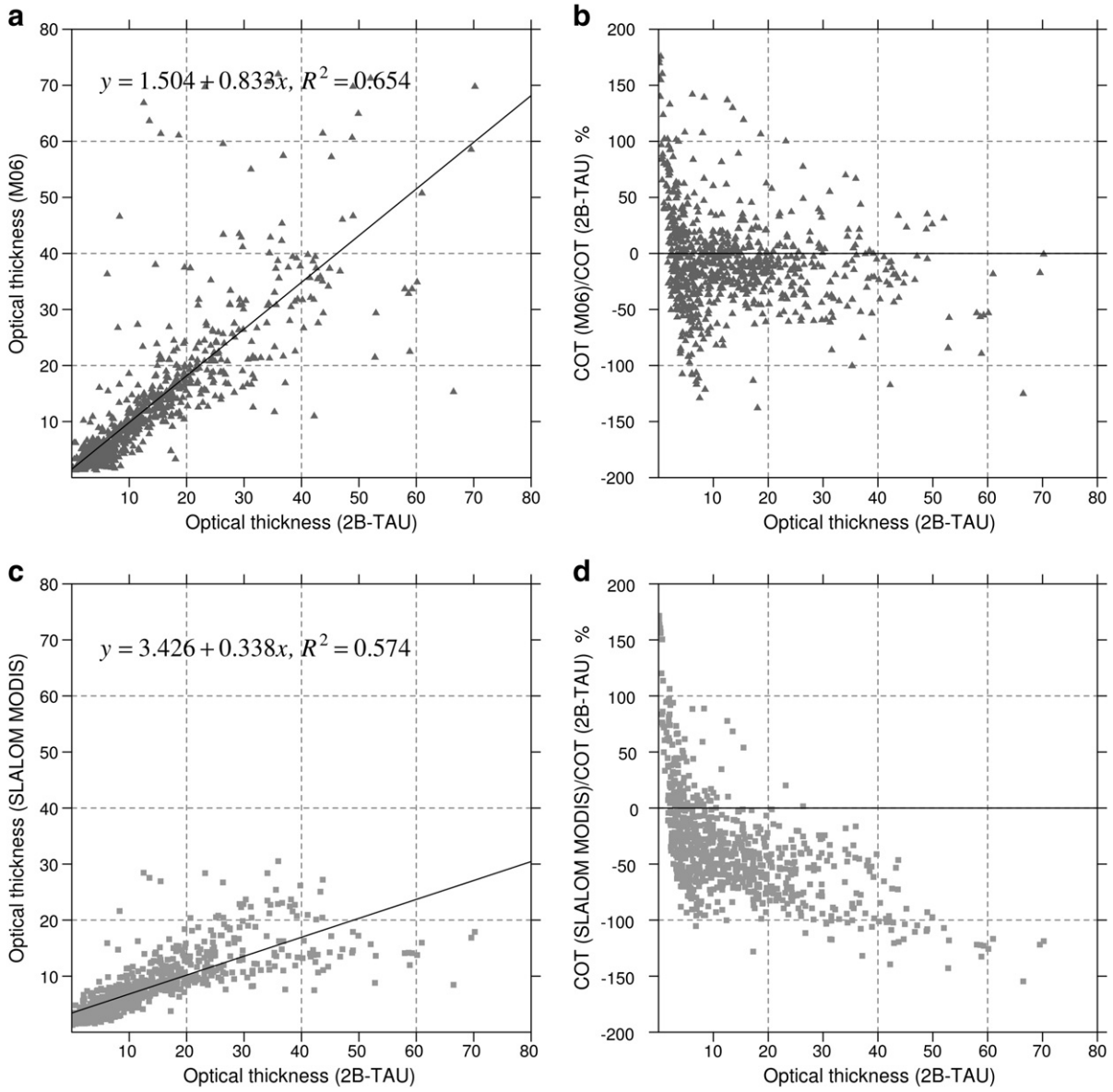

Fig. 19. (a) Cloud optical thickness retrieved by SLALOM using Aqua MODIS data and (c) M06 vs. CloudSat 2B-TAU optical thickness and (b, d) corresponding percentage difference for temporally corresponding Aqua MODIS scenes from Fig. 18.

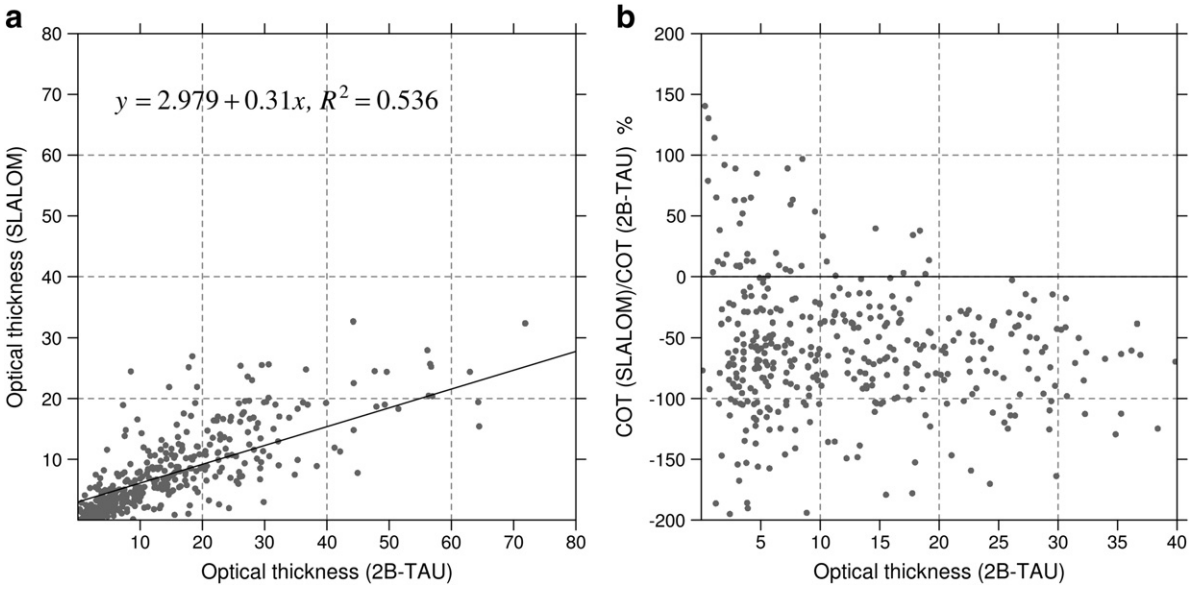

Fig. 20. (a) Cloud optical thickness retrieved by SLALOM using MSG SEVIRI data vs. CloudSat 2B-TAU optical thickness and (b) corresponding percentage difference for Europe scenes from Fig. 18 (mean over all CloudSat profiles within one SEVIRI pixel is taken).

correct the sensor ageing and calibration deficiencies and reduce calibration differences between MSG SEVIRI and MODIS. For the background albedo over land, a minimum composite of the reflectances in the visible (0.65 μm and 0.81 μm) and near-infrared (1.64 μm) channel over one month was calculated. To investigate the performance of SLALOM, the retrievals were evaluated against each other in three steps. First, SLALOM was applied to MODIS data and compared against the MODIS 06 product. Hence both algorithms were applied to the same sensor and differences can be attributed solely to the different assumptions within the retrievals and meta-datasets. Second, SLALOM was applied to MSG SEVIRI data and compared against the MODIS 06 product on a 0.08° by 0.08° grid. The comparison implied potential errors due to different algorithms and additionally potential deviations due to different satellite and sensor characteristics. In the third step, SLALOM-based cloud optical thickness retrieved from MSG SEVIRI and MODIS data as well as MODIS M06 cloud optical thickness were compared to the CloudSat 2B-TAU product. CloudSat provide an accurate cloud optical depth profile and detailed information on the sub-pixel heterogeneity of the cloud structure within the SEVIRI pixel.

Over the Atlantic, $SLALOM_M$ and M06 retrieved cloud properties showed a high level of agreement with coefficients of correlation of 0.99 (τ) and 0.94 (a_{ef}) if pixels with $\tau > 5$ are considered. The rather strong deviations for $a_{efMslalom}$ values around 4 are linked to clouds with $\tau < 10$. The presence of broken clouds and variations between thin and very thin clouds within one pixel may lead to surface visibility at sub-pixel scale resulting in smaller reflectances at 1.6 μm. Based on the cloud reflection function at the absorbing wavelengths, smaller near-infrared reflectances result in larger a_{ef} values. It seems that SLALOM is sensitive to such conditions causing the overestimation. The same effect can be observed in the results over Europe. The correlation coefficient of 0.68 (a_{ef}) increases to 0.89 if values with $\tau < 10$ are excluded. The slightly weaker agreement, which is also apparent for the optical thickness ($r = 0.95$), may be caused by the influence of the background albedo. However, the overall analysis showed very close and comparable results.

When comparing $SLALOM_S$ against M06 on the 0.08° by 0.08° grid, it was noticeable that the range of a_{ef} and τ values is significantly smaller in comparison to the results presented in the SLALOM MODIS/M06 comparison. This may be attributed to the less spatial resolution.

Over the ocean, the retrieved cloud properties showed a good agreement with an r of 0.93 (τ) and 0.82 (a_{ef}). The largest deviations were found in less homogeneous cloud areas that are characterized by broken clouds and along the cloud borders. The different spatial resolution of SEVIRI and MODIS may introduce differences since the retrieved optical properties are based on area-averaged reflectance measurements of about 6 by 8 km (SEVIRI) and 1 by 1 km (MODIS) respectively. At sub-pixel resolution, the homogeneity of a cloud remains unknown. It is also indicated that inhomogeneities are present through large ranges of the CloudSat $\tau_{2B\text{-}TAU}$ values observed within the SEVIRI pixels. Nevertheless, the retrieved $\tau_{Sslalom}$ values are well within the range of the $\tau_{2B\text{-}TAU}$ values that can be found within one SEVIRI pixel, except for the case of very small optical thickness (smaller than 5) where SLALOM tends to overestimate τ. As $\tau_{Sslalom}$ values, τ_{M06} and $\tau_{Mslalom}$ values also correspond very well with CloudSat 2B-Tau which is evident through clear positive correlations with r of 0.95 ($\tau_{Mslalom}$ vs. $\tau_{2B\text{-}TAU}$) and 0.96 (τ_{M06} vs. $\tau_{2B\text{-}TAU}$). In addition, the differences found between $SLALOM_S$ and M06 may be attributed to differences in the calibration of both instruments and the different viewing geometries which subsequently affects the retrieved cloud properties. In order to quantify the differences in the reflectances, a direct comparison of the visible (0.8 μm) and near-infrared (1.6 μm) reflectances of MODIS and SEVIRI was carried out. The variations in SEVIRI and MODIS reflectances showed an acceptable level of agreement with $r = 0.93$ (VIS)

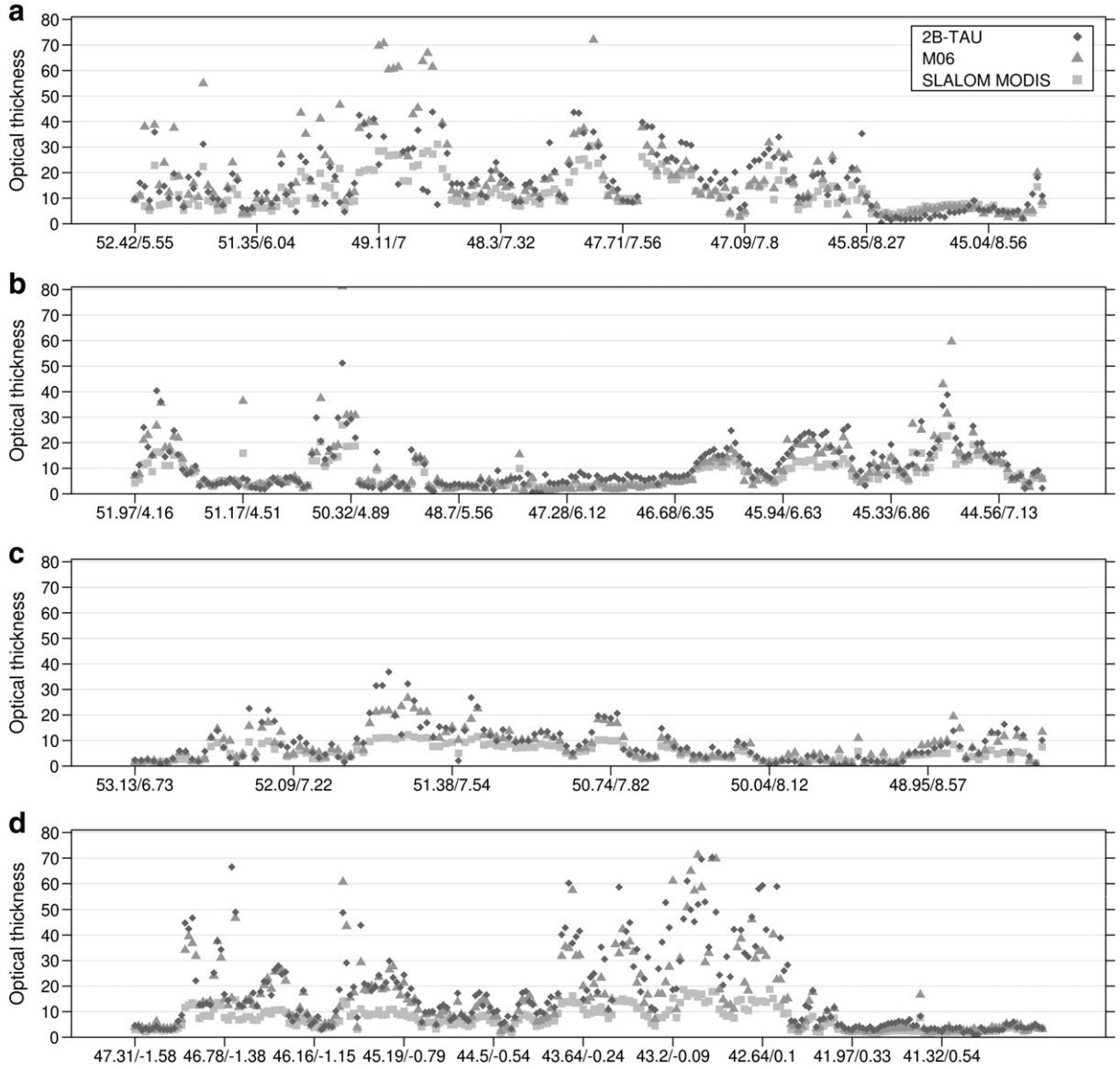

Fig. 21. Cloud optical thickness retrieved by SLALOM using Aqua MODIS data, M06 and CloudSat 2B-TAU optical thickness for temporally corresponding Aqua MODIS scenes from Fig. 18. Retrieved τ values are displayed for each MODIS pixel.

and r = 0.90 (NIR), but the remaining differences may explain the observed differences between $SLALOM_S$ and M06, since the reflection of clouds in the visible region is strongly related to cloud optical thickness, and the cloud droplet radius influences reflection in the near-infrared region. Moreover, even though the datasets were chosen based on minimum time differences between the observations, slight temporal discrepancies may also contribute to differences between the retrievals, as clouds are highly dynamic and their spatio-temporal location and properties can change quickly. Over Germany, the evaluation between $SLALOM_S$ and M06 showed larger differences and the agreement decreased to correlation coefficients of 0.8 and 0.52 for τ and a_{ef} respectively. This can be explained by inhomogeneities of clouds which exhibit quite complex structures particularly over land which are detected on different scales by MODIS and SEVIRI because of their different spatial resolutions. Moreover uncertainties are caused by using different surface albedo products in both retrievals. The presence of significant cloud inhomogeneities was also confirmed through large ranges of $\tau_{2B\text{-}TAU}$ values within many SEVIRI pixels. The likelihood of a mixed cloud scenario being located within a larger SEVIRI pixel is increased. However, the tendency of the $\tau_{2B\text{-}TAU}$ evolution is mapped very well through $\tau_{Sslalom}$. It is conspicuous that for τ larger than 10 values of both SLALOM-based optical thickness products are mainly smaller than the corresponding $\tau_{2B\text{-}TAU}$ values. It seems that the surface albedo has a significant influence on the SLALOM retrieval. τ_{M06} and $\tau_{2B\text{-}TAU}$ values show a good agreement with an r of 0.81.

This paper has demonstrated that the cloud retrieval algorithm SLALOM provides robust estimates of cloud optical

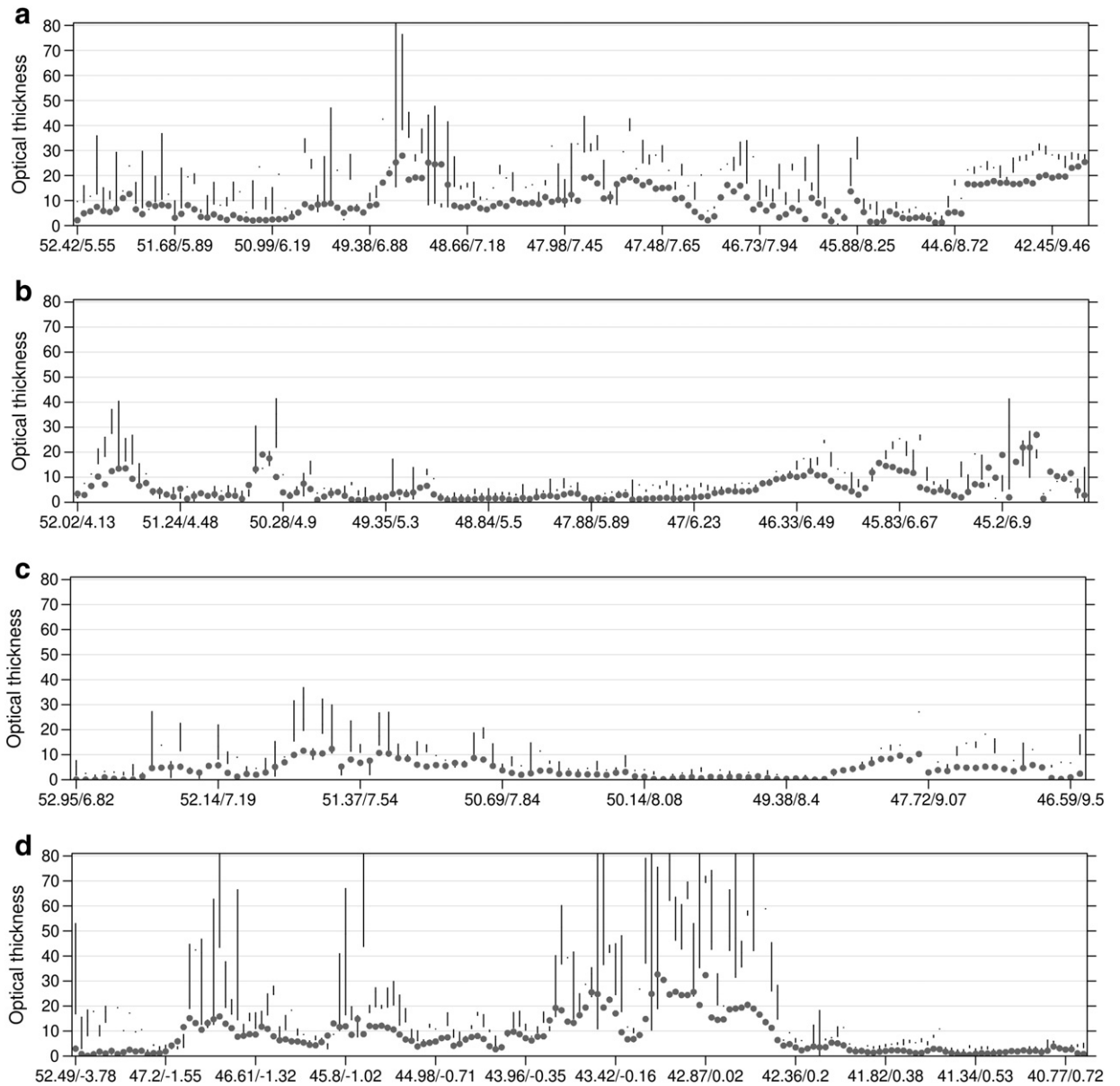

Fig. 22. Cloud optical thickness retrieved by SLALOM using MSG SEVIRI data vs. CloudSat 2B-TAU optical thickness for scenes from Fig. 18. For each SEVIRI pixel the retrieved τ_{Sslalom} value (grey dot) and the range of spatial corresponding $\tau_{\text{2B-TAU}}$ values (black line) are displayed.

thickness and cloud effective radius not only for polar orbiting satellites such as MODIS but also for geostationary satellites such as MSG SEVIRI. The rather simple retrieval technique shows comparable results to the well established NASA products. The inverse problem is solved by approximated analytical equations that enable a fast but hardware-undemanding computation speed. Despite the differences between MSG SEVIRI, Terra/Aqua MODIS and CloudSat with respect to their spectral characteristics, spatial resolutions and viewing geometries, the retrieved cloud properties compare well over the Atlantic. The agreement over land is weaker. We attribute this to (a) uncertainties related to the surface albedo which is treated differently in the algorithms and which is based on different albedo maps and (b) the existence of broken clouds.

Given the demonstrated accuracy of SLALOM using MSG SEVIRI data there is a wide spread of potential applications. Beside a stand-alone application it can be used e.g. in the look-up table codes to generate a first guess or to reject unphysical results. SLALOM could also be used to generate first guess scenarios of physical insights into cloud processes.

Acknowledgments

This work was supported by the Priority Program 1374 “Biodiversity Exploratories” of the German Research Foundation (DFG) Project. The work of A. Kokhanovsky was supported by the ESA Cloud_CCI Project. NASA's CloudSat project products are provided online (www.cloudsat.cira.colostate.edu). The MODIS

data was obtained from NASA's Level 1 and Atmosphere Archive and Distribution System (LAADS web, http://ladsweb.nascom.nasa.gov/). The authors like to thank Jan Fokke Meirink of KNMI for providing MODIS-SEVIRI calibration coefficients. We acknowledge also the support by Rob Roebeling and Sebastien Wagner of EUMETSAT. Furthermore, the authors would like to thank the anonymous reviewers for valuable remarks and comments which helped to improve the manuscript.

References

Aminou, D.M.A., 2002. MSG's SEVIRI instrument. ESA Bull. 111, 15–17.
Arking, A., Childs, J.D., 1985. Retrieval of cloud cover parameters from multispectral satellite images. J. Appl. Meteorol. 24, 322–333.
Bennartz, R., Watts, P., Meirink, J.F., Roebeling, R., 2010. Rainwater path in warm clouds derived from combined visible/near-infrared and microwave satellite observations. J. Geophys. Res. 115 (D19), 1–16. http://dx.doi.org/10.1029/2009JD013679.
Bézy, J.-L., Aminou, D., Bensi, P., Stuhlman, R., Tjemkes, S., Rodriguez, A., 2005. Meteosat Third Generation: the future European Geostationary Meteorological Satellite. ESA Bull. 123, 29–32.
Cermak, J., 2006. SOFOS - A New Satellite-based Operational Fog Observation Scheme. PhD thesis Philipps-Universität Marburg, Fachbereich Geographie, http://archiv.ub.uni-marburg.de/diss/z2006/0149/pdf/djc.pdf.
Cermak, J., Bendix, J., 2008. A novel approach to fog/low stratus detection using Meteosat 8 data. Atmos. Res. 87, 279–292. http://dx.doi.org/10.1016/j.atmosres.2007.11.009.
Feijt, A.J., Jolivet, D., Koelemeijer, R., Deneke, H., 2004. Recent improvements to LWP retrievals from AVHRR. Atmos. Res. 72, 3–15.
Germogenova, T.A., 1963. Some formulas to solve the transfer equation in the plane layer problem. In: Stepanov, B.I. (Ed.), Spectroscopy of Scattering Media. Academy of Sciences of BSSR, Minsk, pp. 36–41.
Govaerts, Y.M., Clerici, M., 2004. Evaluation of radiative transfer simulations over bright desert calibration sites. IEEE Trans. Geosci. Remote. Sens. 42, 176–187.
Greuell, W., Roebeling, R.A., 2009. Toward a standard procedure for validation of satellite-derived cloud liquid water path: a study with SEVIRI data. J. Appl. Meteorol. 48, 1575–1590.
Guenther, B., Godden, G.D., Xiong, X., Knight, E.J., Qiu, S.-Y., Hopkins, M.M., Khayat, M.G., Hao, Z., 1998. Prelaunch algorithm and data format for the level 1 calibration products for the EOS-AM1 Moderate Resolution Imaging Spectroradiometer (MODIS). IEEE Trans. Geosci. Remote. Sens. 36 (4), 1142–1151.
Han, Q., Rossow, W.B., Lacis, A.A., 1994. Near-global survey of effective droplet radii in liquid water clouds using ISCCP data. J. Clim. 7, 465–497.
Im, E., Chialin, Wu., Durden, S.L., 2006. Cloud profiling radar for the CloudSat mission. IEEE Trans. Aerosp. Electron. Syst. 20, 15–18.
Kawamoto, K., Nakajima, T., Nakajima, T.Y., 2001. A global determination of cloud microphysics with AVHRR remote sensing. J. Clim. 14, 2054–2068.
Kiehl, J.T., Trenberth, K.E., 1997. Earth's annual global mean energy budget. Bull. Am. Meteorol. Soc. 78, 197–208.
King, M.D., 1987. Determination of the scaled optical thickness of clouds from reflected solar radiation measurements. J. Atmos. Sci. 44, 1734–1751.
King, M.D., Greenstone, R., 1999. EOS Reference Handbook. Technical Report NASA NP-1999-08-134-GSFC. Goddard Space Flight Center, Greenbelt, MD.
King, M.D., Tsay, S.-C., Platnick, S.E., Wang, M., Liou, K.-N., 1997. Cloud Retrieval Algorithms for MODIS: Optical Thickness, Effective Particle Radius, and Thermodynamic Phase. NASA.
Kokhanovsky, A.A., Nauss, T., 2005. Satellite-based retrieval of ice cloud properties using a semi-analytical algorithm. J. Geophys. Res. 110 (D19), D19206.
Kokhanovsky, A.A., Rozanov, V.V., Zege, P.E., Bovensmann, H., Burrows, J.P., 2003. A semianalytical cloud retrieval algorithm using backscattered radiation in 0.4–2.4 μm spectral region. J. Geophys. Res. 108, 4-1–4-19.
Liou, K.N., 1992. Radiation and cloud processes in the atmosphere. Theory, Observation and Modeling. Oxford University Press, New York.
Liou, K.-N., Wittman, G.D., 1979. Parameterization of the radiative properties of clouds. J. Atmos. Sci. 36, 1261–1273.
Min, Q., Minnis, P., Khaiyer, M.M., 2004. Comparison of cirrus optical thickness depths derived from GOES 8 and surface measurements. J. Geophys. Res. 109, D15207.
Mishchenko, M.I., Dlugach, J.M., Yanovitskij, E.G., Zakharova, N.T., 1999. Bidirectional reflectance of flat, optically thick particulate layers: an efficient radiative transfer solution and applications to snow and soil surfaces. J. Quant. Spectrosc. Radiat. Transf. 63, 409–432.
Munro, R., Ratier, A., Schmetz, J., Klaes, D., 2002. Atmospheric measurements from the MSG and EPS systems. Adv. Space Res. 29, 1609–1618.
Nakajima, T., King, M., 1990. Determination of the optical thickness and effective particle radius of clouds from reflected solar radiation measurements. Part I. Theory. J. Atmos. Sci. 47, 1878–1893.
Nakajima, T.Y., Nakajima, T., 1995. Wide-area determination of cloud microphysical properties from NOAA AVHRR measurements for FIRE and ASTEX regions. J. Atmos. Sci. 52, 4043–4059.
Nauss, T., Kokhanovsky, A.A., 2006. Discriminating raining from nonraining clouds at mid-latitudes using multispectral satellite data. Atmos. Chem. Phys. 6, 5031–5036.
Nauss, T., Kokhanovsky, A.A., 2011. Retrieval of warm cloud optical properties using simple approximations. Remote. Sens. Environ. 115 (6), 1317–1325.
Nauss, T., Kokhanovsky, A.A., Nakajima, T.Y., Reudenbach, C., Bendix, J., 2005. The intercomparison of selected cloud retrieval algorithms. Atmos. Res. 78 (1–2), 46–78. http://dx.doi.org/10.1016/j.atmosres.2005.02.005.
Pandey, P., Ridder, K. De, Gillotay, D., Lipzig, N.P.M., 2012. Estimating cloud optical thickness and associated surface UV irradiance from SEVIRI by implementing a semi-analytical cloud retrieval algorithm. Atmos. Chem. Phys. Discuss. 12, 691–721.
Pérez, J.C., González, A., Armas-Padilla, M., 2011. Remote sensing of water cloud properties from MSG/SEVIRI nighttime imagery. Remote. Sens. Environ. 115, 738–746. http://dx.doi.org/10.1016/j.rse.2010.10.015.
Platnick, S., 2000. Vertical photon transport in cloud remote sensing problems. J. Geophys. Res. 105, 22919–22935.
Platnick, S., Valero, F.P.J., 1995. A validation of a satellite cloud retrieval during ASTEX. J. Atmos. Sci. 52, 2985–3001.
Platnick, S., King, M.D., Ackerman, S.A., Menzel, W.P., Baum, B.A., Riedi, J.C., Frey, R.A., 2003. The MODIS cloud products: algorithms and examples from Terra. IEEE Trans. Geosci. Remote. Sens. 41, 459–473.
Platnick, S., Hubanks, P.A., Wind, G., King, M.D., Ackerman, S.A., Maddux, B., Zinner, T., Ackerman, A., 2009. The MODIS cloud optical and microphysical product: an evaluation of effective radius retrieval statistics and model simulations, hyperspectral imaging and sensing of the environment, OSA technical digest (CD), Optical Society of America, paper HWB1.
Polonsky, I.N., Labonnote, L.C., Cooper, S., 2008. Level 2 Cloud Optical Depth Product Process Description and Interface Control Document, Version 5.0. CloudSat Project, CIRA, Colorado State University, Fort Collins. (21 pp. [Available online at http://www.cloudsat.cira.clostate.edu/ICD/2BTAU/2B-TAU_PDICD_5.0.pdf]).
Roebeling, P.D., Feijt, A.J., Stammes, P., 2006. Cloud property retrievals for climate monitoring: implications of differences between Spinning Enhanced Visible and Infrared Imager (SEVIRI) on METEOSAT-8 and Advanced Very High Resolution Radiometer (AVHRR) on NOAA-17. J. Geophys. Res. 111, D20210. http://dx.doi.org/10.1029/2005JD006990.
Roebeling, R.A., Deneke, H.M., Feijt, A.J., 2008. Validation of cloud liquid water path retrievals from SEVIRI using one year of CloudNET observations. J. Appl. Meteorol. Climatol. 47, 206–222.
Rossow, W., 1989. Measuring cloud properties from space: a review. J. Clim. 2, 201–213.
Schiffer, R.A., Rossow, W.B., 1983. The International Satellite Cloud Climatology Project (ISCCP): the first project of the World Climate Research Programme. Data Manage. 64 (7).
Schmetz, J., Pili, P., Tjemkes, S., Just, D., Kerkmann, J., Rota, S., Ratier, A., 2002. An introduction to Meteosat Second Generation (MSG). Bull. Am. Meteorol. Soc. 83, 977–992.
Schumann, W., Stark, H., McMullan, K., Aminou, D.M.A., Luhmann, H.-J., 2002. The MSG system. ESA Bull. 111, 11–14.
Schutgens, N.A.J., Roebeling, R.A., 2009. Validating the validation: the influence of liquid water distribution in clouds on the intercomparison of satellite and surface observations. J. Atmos. Ocean. Technol. 26, 1457–1474. http://dx.doi.org/10.1175/2009JTECHA1226.1.
Stephans, G.L., Kummerow, C.D., Stephens, G.L., 2007. The remote sensing of clouds and precipitation from space: a review. J. Atmos. Sci. 64, 3742–3765. http://dx.doi.org/10.1175/2006JAS2375.1.
Stephens, G., 2005. Cloud feedbacks in the climate system: a critical review. J. Climate 18, 237–273. http://dx.doi.org/10.1175/JCLI-3243.1.
Stephens, G.L., Vane, D.G., Boain, R.J., Mace, G.G., Sassen, K., Wang, Z., Illingworth, A.J., O'Connor, E.J., Rossow, W.B., Durden, S.L., Miller, S.D., Austin, R.T., Benedetti, A., Mitrescu, C., Cloud Science Team, 2002. The CloudSat mission and the A-Train: a new dimension of space-based observations of clouds and precipitation. Bull. Am. Meteorol. Soc. 83, 1771–1790. http://dx.doi.org/10.1175/BAMS-83-12-1771.
Strabala, K.I., Ackerman, S.A., Menzel, W.P., 1994. Cloud properties inferred from 8–12 μm data. J. Appl. Meteorol. 33, 212–229.
Twomey, S., Cocks, T., 1982. Spectral reflectance of clouds in the near-infrared: comparison of measurements and calculations. J. Meteorol. Soc. Jpn. 60, 583–592.
Zinner, T., Bugliaro, L., Mayer, B., 2005. Remote sensing of inhomogeneous clouds with MSG/SEVIRI. Proceedings of the EUMETSAT Meteorological Satellite Conference 2005. EUMETSAT, Dubrovnik, Croatia, p. 46 (ISBN 92-9110-073-0, ISSN 1011–3932).

Meike Kühnlein received the diploma degree in geography from the Philipps-University of Marburg, Marburg, Germany, in 2008. From 2009 to 2011 she worked as a scientific assistant at the Department of Climatology at Bayreuth University and went on to work as an assistant lecturer in the Environmental Informatics group at the faculty of Geography at University of Marburg, Germany. She is currently working on her Ph.D. thesis focussing on the assignment of rainfall rates to precipitating clouds based on their optical properties derived from multispectral satellite data. Her scientific focus is on atmospheric remote sensing, rainfall and role of clouds in the climate system.

Tim Appelhans graduated with a Diplom in Geography from the Friedrich Alexander University of Erlangen — Nürnberg in 2005. He went on to study climatological influences on air quality in Christchurch New Zealand at the University of Canterbury, Christchurch, New Zealand. In 2010 he received his Doctor of Philosophy in Geography for which he was awarded the President's Award 'Best Doctoral Thesis in Geography' from the New Zealand Geographical Society. In 2011 he joined the Environmental Informatics group at Philipps University Marburg, where he is investigating climatological and anthropogenic influences on biodiversity at Mt. Kilimanjaro, Tanzania.

Boris Thies works as a scientific assistant and lecturer in the Laboratory for Climatology and Remote Sensing at the faculty of Geography at the Philipps-University Marburg. He studied physical geography in Marburg, Germany, where he also received his Ph.D. for developing a rainfall retrieval technique based on multispectral satellite data. His scientific focus is on space borne and ground based remote sensing in climatology and ecology.

Alexander A. Kokhanovsky graduated from the Physical Department of the Belarussian State University, Minsk, Belarus, in 1983. He has received Ph.D. degree in optical sciences from the B. I. Stepanov Institute of Physics, National Academy of Sciences of Belarus, Minsk, Belarus, in 1991. The PhD work was devoted to modeling light scattering properties of aerosol media and foams. His habilitation work (2001) was aimed at cloud and snow remote sensing from space. Alexander Kokhanovsky is currently a member of the SCIAMACHY/ENVISAT algorithm development team (Institute of Environmental Physics, University of Bremen). His research interests are directed toward modeling light propagation and scattering in terrestrial atmosphere. Dr. Kokhanovsky is the author of books *Light Scattering Media Optics: Problems and Solutions* (Chichester: Springer-Praxis, 1999, 2001, 2004), *Polarization Optics of Random Media* (Berlin: Springer-Praxis, 2003), and *Cloud Optics* (Amsterdam: Elsevier, 2006), and *Aerosol Optics* (Berlin: Springer-Praxis, 2008). He published more than 150 papers in the field of environmental optics, radiative transfer, and light scattering.Dr. Kokhanovsky is a member of the American and European Geophysical Unions.

Thomas Nauss received the diploma degree in geography from the University of Munich, Munich, Germany, in 2001, and the Ph.D. degree from the University of Marburg, Marburg, Germany, in 2005. His Ph.D. thesis focussed on the delineation of precipitating clouds based on their optical properties derived from multispectral satellite data. Since 2011 he is professor for Environmental Informatics at the faculty of Geography at the Philipps-University Marburg, Germany. His research interests are directed toward satellite retrievals of cloud properties and precipitation fields.